QUARTERLY OF APPLIED MATHEMATICS

VOLUME LX DECEMBER · 2002 NUMBER 4

DECEMBER 2002, PAGES 601–630

# AN ANALYTICAL STUDY OF THE KELVIN-HELMHOLTZ INSTABILITIES OF COMPRESSIBLE, MAGNETIZED TANGENTIAL VELOCITY DISCONTINUITIES WITH GENERALIZED POLYTROPE LAWS

BY

KEVIN G. BROWN AND S. ROY CHOUDHURY

*Department of Mathematics, University of Central Florida, Orlando, FL*

**Abstract.** The linear Kelvin-Helmholtz instability of tangential velocity discontinuities in high velocity magnetized plasmas with isotropic or anisotropic pressure is investigated. A new analytical technique applied to the magnetohydrodynamic equations with generalized polytrope laws (for the pressure parallel and perpendicular to the magnetic field) yields the complete structure of the unstable, standing waves in the (inverse plasma beta, Mach number) plane for modes at arbitrary angles to the flow and the magnetic field. The stable regions in the (inverse plasma beta, propagation angle) plane are mapped out via a level curve analysis, thus clarifying the stabilizing effects of both the magnetic field and the compressibility. For polytrope indices corresponding to the double adiabatic and magnetohydrodynamic equations, the results reduce to those obtained earlier using these models. Detailed numerical results are presented for other cases not considered earlier, including the cases of isothermal and mixed waves. Also, for modes propagating along or opposite to the magnetic field direction and at general angles to the flow, a criterion is derived for the absence of standing wave instability—in the isotropic MHD case, this condition corresponds to (plasma beta) $\leq 1$.

**1. Introduction.** The Kelvin-Helmholtz (K-H) instability caused by tangential velocity discontinuities in homogeneous plasma is of crucial interest in modeling many problems in space, astrophysical, and geophysical situations involving sheared plasma flows. A detailed understanding of the structure and dynamics of magnetopause regions, such as the presence of the magnetospheric boundary layer and of rapid boundary motions, has been obtained from the recent satellite observations of particles and fields. Many investigators have treated the instability of the interface between the solar wind and the magnetosphere [1]–[5], coronal streamers moving through the solar wind, the

Received January 20, 1998.
2000 *Mathematics Subject Classification.* Primary 76E20, 76E25.
*E-mail address*: choudhur@longwood.cs.ucf.edu

boundaries between the adjacent sectors in the solar wind, the structure of the tails of comets [6], [7], and the boundaries of the jets propagating from the nuclei of extragalactic double radio sources into their lobes [8]–[9]. The linear K-H instability of non-magnetized shear layer has been studied for flows with a subsonic velocity change by Chandrasekhar, Syrovatskii, and Northrop [10], and with an abrupt jump in $v_z$ of arbitrary magnitude by Gerwin [11]. Ray and Ershkovich [12] and Miura [13] have discussed the stability of compressible, magnetized, finite width shear layers for a linear and hyperbolic tangent velocity profile. The K-H instability of a finite width, ideal magnetohydrodynamic shear layer with linear and hyperbolic tangent velocity profiles in the transition region has been discussed by Roy Choudhury and Lovelace, Miura and Pritchett [14], and by Roy Choudhury [15] considering arbitrary magnetic field in $(y, z)$-plane. Uberoi [16] has investigated the finite thickness and angle effects on the marginal instability considering the three layered structure of plasma regions: the magnetosheath, the boundary layer, and the magnetosphere. Fujimoto and Terasawa [17] have carried out the study of ion inertia effect on the K-H instability of two fluids plasma arising from the Hall term. Sharma and Shrivastava [18] have presented the nonlinear analysis of drift K-H instability for electrostatic perturbations. Malik and Singh [19] have studied chaos in the K-H instability in superposed magnetic fluids with uniform relative motion.

In the above studies, most of the treatments used the collision dominated hydromagnetic equations with scalar gas pressure approximation. The scalar gas pressure approximation is not appropriate in dilute plasmas such as the coronal streamers and the solar wind. The plasma in the interplanetary medium, earth's magnetosphere, and the polar exosphere are collisionless. There is a transition zone in solar wind where plasma is neither fully collisional nor collisionless. The K-H instability has been discussed in anisotropic plasma using Chew, Goldberg, and Low (CGL) equations for the situations where collisions are not sufficiently strong to keep the pressure a scalar but sufficiently strong to prevent the heat flow and other transport processes. Roy Choudhury and Patel [20] have considered the K-H instability of an anisotropic, finite width, supersonic shear layer and investigated the nonlocal coupling of the firehose and mirror instabilities via a spatially varying velocity. Duhau et al. [21], [22] have discussed the problem of a tangential velocity discontinuity in a collisionless hydromagnetic region using CGL approximation. Duhau and Gratton [23] have investigated the effect of compressibility on the stability of a vortex sheet in an ideal magnetofluid. Rajaram et al. [24], [25] have examined the contact discontinuities on two collisionless fluids in the magnetosphere across the cusp region of the solar wind magnetosphere boundary. Talwar [26], [27] has presented a study of K-H instability of two streams of homogeneous anisotropic plasma. Pu [28] has developed a new approach called the drift kinetic approximation (DKA) for collisionless space plasmas.

However, more general anisotropic models than the CGL model are necessary in treating low collision regimes, such as in the transitional region of the solar wind. In this connection, we employ the plasma model with generalized polytrope laws for the parallel and perpendicular pressures. This model, proposed by Abraham-Shrauner [29], uses double adiabatic pressure laws with generalized polytrope indices together with the other magnetohydrodynamic (MHD) equations. For specific choices of polytrope indices,

it contains both the MHD and CGL models as special cases. This model has been employed to consider various anisotropic plasma instabilities, including gravitational instability [30], symmetric spherical flow [31], the effects of Hall current and finite electrical resistivity on the magnetogravitational instability [32], and the standing and traveling wave instabilities of anisotropic finite width shear layers [33].

In this paper, we use this model with generalized polytrope laws to investigate the instability of velocity shear layers of zero width analytically and numerically. This generalizes the results obtained in [34] for the instability structure to general polytrope indices, and is able to recover the results derived separately for the CGL and MHD cases in [34] in one, unified formulation (with the choice of the appropriate polytrope indices for each case). In addition to the CGL and MHD cases, we are also able to derive results for the general structure of the standing wave instability for the cases of isothermal and mixed waves.

The remainder of this paper is organized as follows. Section 2 contains the governing equations. Analytic criteria for unstable modes are derived in Section 3. Modes along (or opposite to) the magnetic field are considered in Section 4, while Section 5 treats modes propagating at arbitrary angles to the equilibrium magnetic field and equilibrium velocity. Section 6 re-derives the criterion for standing wave modes in an alternative way.

**2. Anisotropic plasma equations with generalized polytrope laws.** The equations for a compressible inviscid, infinitely conducting plasma are:

$$\begin{aligned}
\rho\frac{d\vec{v}}{dt} &= -\vec{\nabla}\cdot\vec{p} + \frac{1}{4\pi}(\vec{\nabla}\times\vec{\mathrm{B}})\times\vec{\mathrm{B}} \\
\frac{\partial\rho}{\partial t} &= -\vec{\nabla}\cdot(\rho\vec{v}) \\
\frac{\partial\vec{\mathrm{B}}}{\partial t} &= \vec{\nabla}\times(\vec{v}\times\vec{\mathrm{B}}) \\
\vec{\nabla}\cdot\vec{\mathrm{B}} &= 0 \\
\vec{\mathrm{p}} &= \mathrm{p}_\perp\vec{\mathrm{I}} + (\mathrm{p}_\parallel - \mathrm{p}_\perp)\hat{n}\hat{n} \\
\vec{\mathrm{I}} &= \text{unit dyadic}
\end{aligned} \tag{1}$$

and the adiabatic equations of state with generalized polytrope exponents $\alpha$, $\beta$, $\varepsilon$, and $\gamma$ are [29]:

$$\frac{d}{dt}\left(\frac{\mathrm{p}_\parallel B^\alpha}{\rho^\gamma}\right) = 0$$

and

$$\frac{d}{dt}\left(\frac{\mathrm{p}_\perp}{\rho^\varepsilon \mathrm{B}^\beta}\right) = 0.$$

Here, $\parallel$ and $\perp$ denote components parallel and perpendicular to the magnetic field, respectively. For the special choices (a) $\alpha = 0$, $\beta = 0$, $\varepsilon = \frac{5}{3}$, $\gamma = \frac{5}{3}$, $\mathrm{r} = 1$, and (b) $\alpha = 2$, $\beta = 1$, $\varepsilon = 1$, $\gamma = 3$, this model reduces to the MHD and CGL models respectively. The equilibrium we consider (Fig. 1) has a flow velocity $\mathrm{v}_0(x) = v_{0y}(x)\hat{y} + v_{0z}(x)\hat{z}$, a uniform magnetic field $\mathbf{B} = B_0\hat{z}$, constant density $\rho$, and pressures $\mathrm{p}_\parallel$ and $\mathrm{p}_\perp$. In

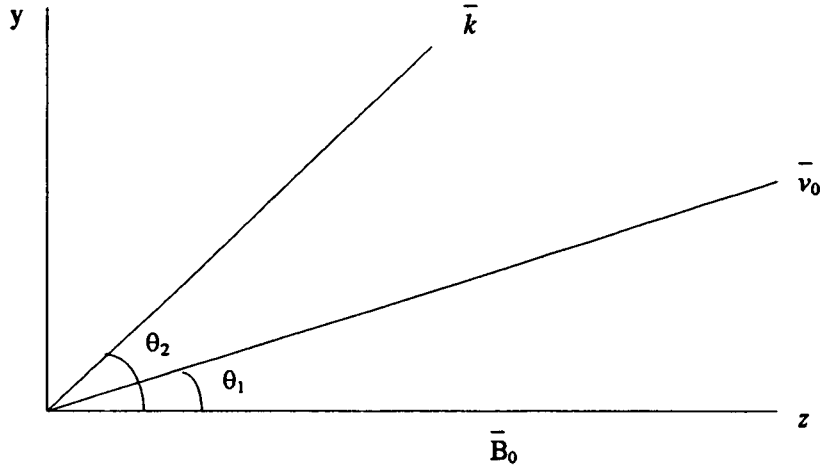


FIG. 1. Geometry of the equilibrium configuration and flow for the compressible tangential velocity discontinuity. The wave vector $\bar{k}$ for the perturbation quantities is shown. Perturbations $\pm\theta_2$ are degenerate.

Section 3 we specialize the velocity to the form $\mathbf{v} = \pm(v_{ym}\hat{y} + v_{zm}\hat{z})$ for $x \neq 0$. Here $\theta_1 = \tan^{-1}\left(\frac{v_{0y}}{v_{0z}}\right)$ is the angle made by the flow velocity with the magnetic field, and $\theta_2 = \tan^{-1}\left(\frac{k_y}{k_z}\right)$ is the angle of propagation of the mode with respect to the magnetic field.

The first order perturbation quantities are of the form $f(x)\exp[i(k_y y + k_z z - \omega t)]$. The frequency $\omega$ is assumed to have at least a small positive imaginary part, so that the solutions correspond to those of an initial-value problem. Linearizing equations (1), we obtain:

$$i\Omega\delta\rho = -\rho(\delta v_x' + ik_y\delta v_y + ik_z\delta v_z), \tag{2a}$$

$$i\Omega\rho\delta v_z + ik_z\delta \mathrm{p}_{\|} + (\mathrm{p}_{\perp} - \mathrm{p}_{\|})ik_z\frac{\delta \mathrm{B}_z}{\mathrm{B}_0} = 0, \tag{2b}$$

$$i\Omega\rho\delta v_x + \delta \mathrm{p}_{\perp}' + \frac{\mathrm{B}_0}{4\pi}\delta \mathrm{B}_z' - \frac{ik_z\mathrm{B}_0}{4\pi}\delta \mathrm{B}_x\left(\frac{\mathrm{p}_{\perp} - \mathrm{p}_{\|}}{\mathrm{B}_0^2/4\pi} + 1\right) = 0, \tag{2c}$$

$$i\Omega\rho\delta v_y + ik_y\delta \mathrm{p}_{\perp} + \frac{ik_y\mathrm{B}_0}{4\pi}\delta \mathrm{B}_z - \frac{ik_z\mathrm{B}_0}{4\pi}\delta \mathrm{B}_y\left(\frac{\mathrm{p}_{\perp} - \mathrm{p}_{\|}}{\mathrm{B}_0^2/4\pi} + 1\right) = 0, \tag{2d}$$

$$\frac{\delta \mathrm{p}_{\perp}}{\mathrm{p}_{\perp}} = \varepsilon\frac{\delta\rho}{\rho} + \beta\frac{\delta \mathrm{B}_z}{\mathrm{B}_0}, \tag{2e}$$

$$\frac{\delta \mathrm{p}_{\|}}{\mathrm{p}_{\|}} = \gamma\frac{\delta\rho}{\rho} - \alpha\frac{\delta \mathrm{B}_z}{\mathrm{B}_0}, \tag{2f}$$

$$i\Omega\delta \mathrm{B}_x = ik_z\mathrm{B}_0\delta v_x, \tag{2g}$$

$$i\Omega\delta \mathrm{B}_y = ik_z\mathrm{B}_0\delta v_y + \mathrm{S}v_0'\delta \mathrm{B}_x, \tag{2h}$$

$$i\Omega\delta B_z = ik_z B_0 \delta v_z + C v_0' \delta B_x - B_0[\delta v_x' + ik_y \delta v_y + ik_z \delta v_z], \tag{2i}$$

$$\delta B_x' + ik_y \delta B_y + ik_z \delta B_z = 0. \tag{2j}$$

Here the prime denotes a derivative with respect to $x$, $C \equiv \cos(\theta_1)$, $S \equiv \sin(\theta_1)$, and $\Omega \equiv (k_y v_0 S + k_z v_0 C - \omega)$. The equilibrium quantities are $p_\parallel$, $p_\perp$, $\rho$, and $v_0(x)$.

Now, what we wish to do is to take these linearized equations and combine them into one equation that is dependent upon one variable only. Since we want to ensure that none of the physical properties are lost, we shall make use of all the equations in the process. The resulting composite equation is [33]:

$$\frac{i\rho\Omega^2 \delta B_x}{k_z B_0} + p_\perp \left[\frac{i\varepsilon(\chi_2 \delta B_z + \chi_3 \delta B_z)}{\Omega} + \beta \frac{\delta B_z}{B_0}\right]' - \frac{B_0}{4\pi}[\chi_7(\delta B_x' + ik_y \chi_4 \delta B_x)]' - \frac{ik_z B_0}{4\pi}\left(\frac{p_\perp - p_\parallel}{B_0^2/4\pi} + 1\right)\delta B_x = 0, \tag{3}$$

where $\delta B_z$ is given by

$$\delta B_z = -\chi_7(\delta B_x' + ik_y \chi_4 \delta B_x). \tag{4}$$

Here, we use the symbols

$$\chi_1 = ik_z^2\{(1+\alpha)p_\parallel - p_\perp\} - i\rho\Omega^2, \tag{5a}$$

$$\chi_2 = \rho\Omega C Q v_0', \tag{5b}$$

$$\chi_3 = Q\chi_1, \tag{5c}$$

$$Q = \left[\rho\Omega B_0 - \frac{\gamma k_z^2 B_0 p_\parallel}{\Omega}\right]^{-1}, \tag{5d}$$

$$\chi_6 = ik_z^2\left(p_\perp - p_\parallel + \frac{B_0^2}{4\pi}\right) - i\rho\Omega^2, \tag{5e}$$

$$\chi_5 = \frac{\left[-\frac{\varepsilon k_y k_z B_0 p_\perp \chi_3}{\Omega} + \frac{ik_y k_z B_0^2}{4\pi} + ik_y k_z p_\perp \beta\right]}{\chi_6} \quad \text{or} \tag{5f}$$

$$\chi_5\chi_6 = -\frac{\varepsilon k_y k_z B_0 p_\perp \chi_3}{\Omega} + \frac{ik_y k_z B_0^2}{4\pi} + ik_y k_z p_\perp \beta,$$

$$\chi_4 = \frac{\left[-\frac{\varepsilon k_y k_z B_0 p_\perp \chi_2}{\Omega} - \rho\Omega S v_0'\right]}{\chi_6} \quad \text{or} \quad \chi_4\chi_6 = -\frac{\varepsilon k_y k_z B_0 p_\perp \chi_2}{\Omega} - \rho\Omega S v_0', \tag{5g}$$

$$\chi_7 = (ik_y\chi_5 + ik_z)^{-1}. \tag{5h}$$

Notice that we have used all the perturbation equations (2) in deriving Eq. (3). Also notice that all the physical quantities characterizing the perturbation ($\delta v$, $\delta B$, $\delta\rho$, $\delta p_\parallel$, $\delta p_\perp$) may be obtained in terms of $\delta B_x$ evaluated from Eq. (3). For the polytrope indices $\alpha = 2$, $\beta = \varepsilon = 1$, and $\gamma = 3$ corresponding to the CGL model, Eq. (3) reduces to Eq. (4) of [34].

The singular points of Eq. (3), as well as the regimes of hyperbolic and elliptic behavior of the equation external to the region of velocity shear, are analogous to the earlier discussion for modes propagating parallel to both the magnetic field and the flow [20].

Outside the region of velocity shear (in the infinite medium: for the vortex sheet, this corresponds to $x > 0$ or $x < 0$), $v_0 =$ constant. For $k_y = 0$ and $\theta_1 = 0$, Eq. (3)

reduces to Eq. (18) of [27] for the CGL polytrope indices $\alpha = 2$, $\beta = \varepsilon = 1$, and $\gamma = 3$, and when Eq. (2g) is used. In the absence of velocity shear, $\frac{d^2}{dx^2} = -k_x^2$ and we recover the dispersion relation for Alfvén wave propagation in a static, infinite, homogeneous, anisotropic plasma [35]. This leads to firehose and mirror instabilities, with these modes being coupled when velocity shear is included. For nonzero values of $k_y$ and $\theta_1$, external to the region of velocity shear, Eq. (3) reduces to:

$$i\chi_{7+}k_z\left[\varepsilon+\beta+\mathrm{q_D^2}+\frac{\varepsilon\{(\gamma-1-\alpha)\mathrm{r}^2+1\}}{\mathrm{u_{D\pm}^2}-\gamma\mathrm{r}^2}\right]\delta\mathrm{B}_x'+k_z^2[u_{D\pm}^2-(1-r^2+q_D^2)]\delta\mathrm{B}_z=0,$$

where we have used the fact that $\chi_2 = \chi_4 = 0$ for $v_0 =$ constant. The $\pm$ subscripts denote the two sides external to the region of velocity shear. This equation has solutions $\delta\mathrm{B}_x = \text{constant}\exp(\pm ik_- x)$ and $\delta\mathrm{B}_x = \text{constant}\exp(\pm ik_+ x)$ in the two external regions, where,

$$k_\pm^2=\frac{k_z^2[(u_{D\pm}^2-\gamma r^2)\{u_{D\pm}^2-(1-r^2+q_D^2)\}-T^2\{(\beta+q_D^2)(u_{D\pm}^2-\gamma r^2)-\varepsilon((1+\alpha)r^2-1-u_{D\pm}^2)\}]}{(\beta+\varepsilon+q_D^2)(u_{D\pm}^2-\gamma r^2)+\varepsilon\{(\gamma-1-\alpha)r^2+1\}}. \tag{6}$$

Here, $\mathrm{T} = \tan\theta_2 = \left(\frac{k_y}{k_z}\right)$ and $\theta_2$ is the angle of propagation of the mode to the magnetic field. Perturbations $\pm\theta_2$ are equivalent, and only positive $\theta_2$ values are considered. In a reference frame comoving with the fluid, Eq. (6) is simply the dispersion relation for sound waves propagation along the magnetic field, and for the firehose and mirror modes [20], [36]. Here, we introduce the *dimensionless frequency*

$$\mathrm{W} \equiv \frac{\omega}{k_z \mathrm{S}_\perp} = \mathrm{W_r} + i\mathrm{W_i}, \tag{7a}$$

and the *dimensionless flow velocity*

$$\mathrm{u_D} = \frac{\Omega}{k_z \mathrm{S}_\perp} = \pm\frac{\mathrm{MF}}{2} - \mathrm{W_D}, \tag{7b}$$

where $\mathrm{S}_{\parallel,\perp} \equiv \left(\frac{\mathrm{p}_{\parallel,\perp}}{\rho}\right)^{\frac{1}{2}}$ are the sound speeds parallel and perpendicular to the magnetic field. We also define the *dimensionless anisotropy parameter*

$$\mathrm{r} = \frac{\mathrm{S}_\parallel}{\mathrm{S}_\perp}, \tag{7c}$$

and the ratio of the magnetic field-energy density to the perpendicular thermal energy density (the *inverse plasma beta*)

$$\mathrm{q_D^2} \equiv \left(\frac{v_\mathrm{A}}{\mathrm{S}_\perp}\right)^2, \tag{7d}$$

where the Alfvén speed is

$$v_\mathrm{A}^2 \equiv \frac{\mathrm{B}_0^2}{4\pi\rho}. \tag{7e}$$

In the external regions, the full dependencies are

$$\delta\mathrm{B}_x = \text{constant}\exp[i(\pm k_- x + k_y y + k_z z - \omega t)]$$

and

$$\delta\mathrm{B}_x = \text{constant}\exp[i(\pm k_+ x + k_y y + k_z z - \omega t)]$$

on the two sides of the region of velocity shear. Here, $\omega = \omega_r + i\omega_i$, in general, with $\omega_i > 0$ for unstable wave solutions. The correct choice of the $\pm$ signs in the external regions is determined by dual considerations. The $x$ component of the magnetic field perturbation $\delta B_x$ should correspond to a spatially damping (in $x$), and outgoing mode at $x \to \pm\infty$ in the comoving frame of the plasma in each of the external regions [14]. The solutions for $k_\pm^2$ in Eq. (6) may be considered in an analogous manner to earlier work [14], [20], applying these criteria. However, this will not be necessary in the remainder of this paper.

**3. Solutions for three-dimensional anisotropic vortex sheet.** We now consider an anisotropic velocity discontinuity (vortex sheet), $v_0 = \pm(v_{ym}\hat{y} + v_{zm}\hat{z})$ for $x > 0$ and $x < 0$. In order to treat this case, the straightforward approach is to start with the perturbation equations (2) and match quantities on the two sides of the discontinuity at $x = 0$ so as to satisfy the boundary conditions [10]: i) the normal velocity is continuous; ii) the normal magnetic field is continuous; and iii) the normal total, Reynolds' (fluid) plus Maxwell (electromagnetic), stress is continuous across the interface. However, the dispersion relation obtained in this manner is more easily derived by integrating the composite Eq. (3) across the discontinuity at $x = 0$. In performing the integration, it is necessary to remember that all quantities are continuous across the jump, with the exception of $v_0$, so that $\left(\frac{dv_0}{dx}\right)$ contains a Kronecker delta. This procedure automatically takes into account the boundary conditions mentioned above, as may be explicitly verified, since all the perturbation equations (2) are incorporated in (3).

Integrating (3) across the jump at $x = 0$, and denoting quantities for $x > 0$ and $x < 0$ respectively by subscripts $+$ and $-$ as before, we obtain

$$\chi_{7+}\delta B_x' \left[p_\perp \left(\frac{i\varepsilon\chi_3}{\Omega} + \frac{\beta}{B_0}\right) + \frac{B_0}{4\pi}\right]_+ = \chi_{7-}\delta B_x' \left[p_\perp \left(\frac{i\varepsilon\chi_3}{\Omega} + \frac{\beta}{B_0}\right) + \frac{B_0}{4\pi}\right]_- , \tag{8a}$$

which reduces to

$$\begin{aligned} \chi_{7+}k_+ &\left[\varepsilon + \beta + q_D^2 + \frac{\varepsilon\{(\gamma - 1 - \alpha)r^2 + 1\}}{u_{D+}^2 - \gamma r^2}\right] \\ &= \pm\chi_{7-}k_- \left[\varepsilon + \beta + q_D^2 + \frac{\varepsilon\{(\gamma - 1 - \alpha)r^2 + 1\}}{u_{D-}^2 - \gamma r^2}\right], \end{aligned} \tag{8b}$$

where we have used the fact that $\delta B_x = \text{constant} \exp\{-ik_\pm x\}$ on the two sides of the discontinuity. For the CGL values of the polytrope indices, $\varepsilon = \beta = 1$, $\alpha = 2$, and $\gamma = 3$, Eq. (8b) reduces to exactly Eq. (7a) of [34]. For modes propagating parallel or antiparallel to the magnetic field $\theta_2 = 0$, $\pi(k_y = 0$ or $T = 0)$, and Eq. (8b) reduces to

$$\begin{aligned} k_+ &\left[\varepsilon + \beta + q_D^2 + \frac{\varepsilon\{(\gamma - 1 - \alpha)r^2 + 1\}}{u_{D+}^2 - \gamma r^2}\right] \\ &= \pm k_- \left[\varepsilon + \beta + q_D^2 + \frac{\varepsilon\{(\gamma - 1 - \alpha)r^2 + 1\}}{u_{D-}^2 - \gamma r^2}\right]. \end{aligned} \tag{8c}$$

The $+$ sign is picked on the right-hand sides of equations (8) since the correct spatially damping and outgoing solutions (in the comoving frame) on the two sides are $\delta B_x =$

constant $\exp(-ik_{\pm}x)$ [20]. However, in practice, the dispersion relation Eq. (8b) or (8c) is squared in order to obtain solutions. The solutions are then "tested out" by substituting back into equations (8) and the spurious solutions introduced by squaring are discarded [14]. The spurious solutions may also be identified since their growth rates do not vanish when one lets the velocity discontinuity tend to zero.

For the vortex sheet velocity profile,

$$\mathrm{u_D} = \pm\frac{\mathrm{MF}}{2} - \mathrm{W_D}, \tag{9a}$$

where

$$\mathrm{F} = \frac{\cos(\theta_1 - \theta_2)}{\cos\theta_2}. \tag{9b}$$

For $\theta_1 = \theta_2 = 0$, $\mathrm{F} = 1$. For $\theta_2 = 0$, $\mathrm{F} = \cos\theta_1$. Here,

$$\mathrm{M} \equiv (\text{velocity discontinuity } /\mathrm{S}_{\perp}) = \left(\frac{2v_0}{\mathrm{S}_{\perp}}\right) \tag{10}$$

is the Mach number of the anisotropic vortex sheet.

**A. Modes propagating parallel or antiparallel to the magnetic field.** Squaring and solving Eq. (8c) for $\theta_2 = 0$ ($k_y = 0$ or $\mathrm{T} = 0$), employing Eq. (9a) in the solution, and picking out the valid solution, one recovers a generalized form of Eq. (27) of [27] for $\theta_1 \neq 0$ ([27] uses $\theta_1 = 0$). The difference due to $\theta_1 \neq 0$ is that M is changed to $\mathrm{M}\cos\theta_1$ everywhere. Therefore, the criteria for unstable traveling and standing wave instability, for modes propagating along or opposite to the magnetic field direction, are given by inequalities (12) of [20] with M replaced by $\mathrm{M}\cos\theta_1$, and q replaced by $\mathrm{q_D}$ (from the change in notation) everywhere.

**B. $|\mathrm{W_D}| \ll \mathrm{MF}$ solutions.** Squaring Eq. (8b) (for general values of $\theta_1$ and $\theta_2$) and using Eq. (6) for $k_{\pm}^2$ we obtain the dispersion relation for modes propagating at arbitrary angles to the flow and the magnetic field:

$$\begin{aligned}&\frac{[(\beta+\varepsilon+q_D^2)(u_{D+}^2-\gamma r^2)+\varepsilon\{(\gamma-1-\alpha)r^2+1\}](1-\mathrm{r}^2+q_D^2-u_{D+}^2)^2}{[(1-\mathrm{r}^2+q_D^2-u_{D+}^2)(u_{D+}^2-\gamma r^2)+\mathrm{T}^2\{(\beta+q_D^2)(u_{D+}^2-\gamma r^2)-\varepsilon((1+\alpha)r^2-1-u_{D+}^2)\}]}\\ &=\frac{[(\beta+\varepsilon+q_D^2)(u_{D-}^2-\gamma r^2)+\varepsilon\{(\gamma-1-\alpha)r^2+1\}](1-\mathrm{r}^2+q_D^2-u_{D-}^2)^2}{[(1-\mathrm{r}^2+q_D^2-u_{D-}^2)(u_{D-}^2-\gamma r^2)+\mathrm{T}^2\{(\beta+q_D^2)(u_{D-}^2-\gamma r^2)-\varepsilon((1+\alpha)r^2-1-u_{D-}^2)\}]}.\end{aligned} \tag{11}$$

For the CGL values of the polytrope indices, $\varepsilon = \beta = 1$, $\alpha = 2$, and $\gamma = 3$, Eq. (11) reduces to exactly Eq. (10) of [34]. Substituting Eq. (9a) in Eq. (11), we obtain an equation which is quadratic in $\mathrm{W_D^2}$ (ignoring the trivial $\mathrm{W_D} = 0$ solution). Therefore, in general, a solution would require the use of the roots of a quartic equation. This is unlike the case for $\theta_2 = 0$ when a fourth-order equation (a biquadratic) in $\mathrm{W_D}$ results. For this case, the roots of the quartic (in $\mathrm{W_D^2}$) Eq. (11) yielded seventy-two pages of *Mathematica* output, making it virtually impossible to distinguish the genuine solutions from the spurious ones introduced by squaring Eq. (8b) to obtain Eq. (11). However, guided by the consideration that $|\mathrm{W_D}| \ll \mathrm{MF}$ for the unstable standing wave solutions in the case with $\theta_1 = \theta_2 = 0$ [20], we look for unstable solutions of Eq. (11) satisfying

the inequality $|W_D| \ll MF$. The validity of this inequality is justified *a posteriori*. This approach turns out to be very fruitful. It results in simple, general analytical solutions for the unstable standing models of Eq. (11).

For $|W_D| \ll MF$, using Eq. (9a) we expand $u_{D\pm}^2 \approx \frac{M^2F^2}{4} \mp MFW_D$. Substituting these equations in Eq. (11), we obtain

$$b_5 W_D^4 - b_3 W_D^2 + b_1 = 0, \tag{12a}$$

where

$$\begin{aligned}
b_5 &= M^4F^4\psi_1, \\
b_3 &= M^2F^2\psi_2\psi_3 + M^2F^2\psi_1\psi_3^2 - \varepsilon M^2F^2\psi_2 T^2 + 2\varepsilon M^2F^2\psi_1\psi_3 T^2 \\
&\quad - M^2F^2\psi_2\psi_4 T^2 + 2M^2F^2\psi_1\psi_3\psi_4 T^2 - M^2F^2\psi_1\psi_5 T^2 \\
&\quad + M^2F^2\psi_2 X - \varepsilon M^2F^2\psi_1 T^2 X + M^2F^2\psi_1 X^2, \\
b_1 &= \psi_2\psi_3^3 + \varepsilon\psi_2\psi_3^2 T^2 + \psi_2\psi_3^2\psi_4 T^2 - 2\psi_2\psi_3\psi_5 T^2 + \psi_1\psi_3^2\psi_5 T^2 \\
&\quad + \psi_2\psi_3^2 X + \varepsilon\psi_1\psi_3^2 T^2 X + 2\psi_2\psi_3\psi_4 T^2 X - 2\psi_1\psi_3\psi_5 T^2 X \\
&\quad + \psi_1\psi_3^2 X^2 + 2\psi_1\psi_3\psi_4 T^2 X^2,
\end{aligned} \tag{12b}$$

and

$$\begin{aligned}
X &= \frac{M^2F^2}{4} - \gamma r^2, \\
\psi_1 &= \beta + \varepsilon + q_D^2, \\
\psi_2 &= \varepsilon\{(\gamma - 1 - \alpha)r^2 + 1\}, \\
\psi_3 &= 1 - r^2 + q_D^2 - \frac{M^2F^2}{4}, \\
\psi_4 &= \beta + q_D^2, \\
\psi_5 &= \varepsilon\left\{(1+\alpha)r^2 - 1 - \frac{M^2F^2}{4}\right\}.
\end{aligned} \tag{12c}$$

Therefore,

$$W_D^2 = \left[b_3 - \sqrt{b_3^2 - 4b_1b_5}\right]/2b_5. \tag{13}$$

Here we have omitted the spurious solution introduced by squaring the dispersion relation (8b). One must check that $|W_D|$ (given by Eq. (13)) $\ll MF$. Here, $|W_D|$ may be maximized with respect to MF, $\theta_1$, and $\theta_2$ using Eq. (13). However, we will not pursue this here. For unstable standing waves ($W_{Dr} = 0, W_{Di} > 0$), we require $W_D^2$ to be real and negative. For $b_3 < 0$ this is satisfied if $b_3^2 > 4b_1b_5$. Therefore, we require $(b_1b_5) < 0$ for $b_5 > 0$ and $(b_1b_5) > 0$ for $b_5 < 0$ with the expression under the square root in Eq. (13) being positive. The criteria for unstable standing wave solutions in Eq. (13) are therefore, since $b_5 > 0$ under the assumption $|W_D| \ll MF$,

(i) $\quad b_1 < 0$ only if $b_3 > 0$

and

(ii) $\quad b_3^2 > 4b_1b_5,$ (14a)

which may be written as

$$\begin{aligned}\psi_3\{\psi_3[\psi_1 X^2 + \psi_2(X + \psi_3)] + [2\psi_1(\psi_1 - \varepsilon)X^2 \\ + (\varepsilon\psi_1\psi_3 + 2\psi_1\psi_2 - 2\varepsilon\psi_2 - 2\psi_1\psi_5)X \\ + (\psi_1\psi_2\psi_3 - 2\psi_2\psi_5 + \psi_1\psi_3\psi_5)]T^2\} < 0\end{aligned} \tag{14b}$$

and

$$\begin{aligned}&[M^2F^2\psi_2\psi_3 + M^2F^2\psi_1\psi_3^2 - \varepsilon M^2F^2\psi_2T^2 + 2\varepsilon M^2F^2\psi_1\psi_3T^2 - M^2F^2\psi_2\psi_4T^2 \\ &\quad + 2M^2F^2\psi_1\psi_3\psi_4T^2 - M^2F^2\psi_1\psi_5T^2 + M^2F^2\psi_2X \\ &\quad - \varepsilon M^2F^2\psi_1T^2X + M^2F^2\psi_1X^2]^2 \\ &\quad > 4M^4F^4\psi_1[\psi_2\psi_3^3 + \varepsilon\psi_2\psi_3^2T^2 + \psi_2\psi_3^2\psi_4T^2 - 2\psi_2\psi_3\psi_5T^2 + \psi_1\psi_3^2\psi_5T^2 \\ &\quad + \psi_2\psi_3^2X + \varepsilon\psi_1\psi_3^2T^2X + 2\psi_2\psi_3\psi_4T^2X - 2\psi_1\psi_3\psi_5T^2X + \psi_1\psi_3^2X^2 \\ &\quad + 2\psi_1\psi_3\psi_4T^2X^2].\end{aligned} \tag{14c}$$

Inequalities (14) will be used to map out the structure of the unstable standing modes in the $(MF, q_D)$ plane. For the CGL polytrope index values $\varepsilon = \beta = 1$, $\alpha = 2$, and $\gamma = 3$, inequalities (14) reduce to inequalities (13) of [34]. Subsequently, in Section 6 we prove analytically for the special case $\theta_2 = 0$ that the criterion (14b) for instability is in fact the general condition for standing wave instability without making the assumption $|W_D| \ll MF$ considered here. Note that, for other values of $\theta_1$ and $\theta_2$, inequality (14b) yields the criterion for standing wave instability.

**C. Criteria for stability and search for the most unstable directions of propagation.** In applications in astrophysics and geophysics, we are not particularly interested in stability information along a specific direction ($\theta_2$) of the propagation vector $\bar{k}$ (to $\bar{B}_0$). Of greater interest [37], is (a) which directions of propagation are unstable, and (b) whether flow parameters exist for which the tangential velocity discontinuity is stable for all propagation directions $\theta_2$. To consider these issues in detail, let us look first for the conditions when no unstable standing waves exist, i.e., $W_D^2$ in (13) is real and positive. From (13) and noting that $b_5 > 0$, the conditions for stable standing waves are

(i) $b_1 > 0$,
(ii) $b_3 > 0$, and
(iii) $b_3^2 - 4b_1b_5 > 0$,

with the $b_i$'s given by (12b). Although $b_1$ and $b_3$ are, respectively, quartic and cubic in $(MF)^2$, $b_3^2 - 4b_1b_5$ contains $(MF^2)^6 = M^6F^{12}$. Thus, the inequalities are impossible to solve in closed form. Instead, for any set of polytrope indices $\alpha$, $\beta$, $\varepsilon$, and $\gamma$, and chosen values of the anisotropy parameter r and $\lambda = M\cos(\theta_2 - \theta_1)$ (so that $MF = M\cos(\theta_2 - \theta_1)/\cos\theta_2 = \lambda\sqrt{1 + T^2}$), we shall map out the region of $(q_D, \theta_2)$-space where the inequalities are satisfied, so that no unstable standing wave modes exist. The boundary of the stable region in $(q_D, \theta_2)$ space will be given by the zero level curves of $b_1, b_3$, and $b_3^2 - 4b_1b_5$, i.e., the curves $b_1 = 0$, $b_3 = 0$, and $b_3^2 - 4b_1b_5 = 0$. The stable region of $(q_D, \theta_2)$-space will be that on the positive side of all three zero level curves, where all three inequalities are satisfied.

Before presenting the results of doing this, let us recover the classical fluid mechanical result for the stable region [10], [11]. For the unmagnetized fluid-mechanical case with an adiabatic law for the energy equation, $q_D = 0$, r = 1, $\alpha = \beta = 0$, $\varepsilon = \gamma = \frac{5}{3}$. Since there is no magnetic field, the angle $\theta_2$ of the model $\bar{k}$ to the magnetic field is arbitrary. Picking $\theta_2 = 0$ implies $F = \cos\theta_1$ and $T = 0$. With all of the above, the conditions $b_1 > 0$, $b_3 > 0$, and $b_3^2 - 4b_1b_5 > 0$ for stability yield (after some algebra) $M^2\cos^2\theta_1 > \frac{40}{3}$ and $M^2\cos^2\theta_1 > \frac{20}{3}$. Using the more restrictive condition $M^2\cos^2\theta_1 > \frac{40}{3}$, together with $M = \frac{v_0}{S_\perp}$, and $S_\perp^2 = \frac{c_s^2}{\gamma} = \frac{3c_s^2}{5}$ ($c_s$ is the adiabatic sound speed), yields

$$\cos\theta_1 > \frac{2\sqrt{2}c_s}{v_0},$$

which is the classical fluid dynamical stability criterion [10], [11], [37].

Returning now to delineating the stable regions of $(q_D, \theta_2)$-space for more general cases, we employ the zero level curves of $b_1$, $b_3$, and $b_3^2 - 4b_1b_5$ as discussed above for each set of $\alpha$, $\beta$, $\varepsilon$, $\gamma$, r, and $\lambda = M\cos(\theta_2 - \theta_1)$. In all the figures in this subsection the stable region of the $(q_D, \theta_2)$-plane is the white space.

Figures 2 through 5 are for the CGL indices ($\alpha = 2, \beta = \varepsilon = 1, \gamma = 3$). In Fig. 2, the tangential discontinuity is unstable for all $q_D$ for $\theta_2 > 1.47$. Figures 2 to 4 show the effect (for $\lambda = 2$) of increasing the anisotropy parameter r from 0.1 to 2 and then to 10. Roughly speaking, the stable region shrinks as r is increased. In Figures 2 to 4, note the unstable (black) band near $\theta_2 = \frac{\pi}{2}$. This is because the first stabilizing effect, due to the magnetic field, is weakest near $\theta_2 = \frac{\pi}{2}$ and vanishes for $\bar{k}\cdot\bar{B}_0 = 0$ or $\theta_2 = \frac{\pi}{2}$.

However, Fig. 5 (which has r = 10 as for Fig. 4) where $\lambda$ has been increased from 2 to 10 demonstrates the other stabilizing effect, that due to compressibility (finite sound speed $c_s$). Now the narrow unstable region near $\theta_2 = \frac{\pi}{2}$ in Fig. 4 (for small $q_D$) has been stabilized by the increased $\lambda$. The classical hydrodynamics stability result $\cos\theta_1 > \frac{2^{3/2}c_s}{v_0}$ derived above has an MHD counterpart [38], which implies that for $(\theta_2 - \theta_1)$ large enough (or $\lambda = M\cos(\theta_2 - \theta_1)$ small enough), no stabilization due to compressibility results. However, as $(\theta_2 - \theta_1)$ decreases (or $\lambda$ increases), stabilization due to compressibility occurs as seen for small $q_D$ near $\theta_2 = \frac{\pi}{2}$ in Fig. 5. Note that there is no stabilization due to the magnetic field line tension at $\theta_2 = \frac{\pi}{2}$. We have verified that as $\lambda$ is increased further, the unstable (black) region of $(q_D, \theta_2)$-space shrinks further, although the results are not shown.

Figures 6 to 8 are for the MHD case ($\alpha = \beta = 0, \varepsilon = \gamma = \frac{5}{3}$, r = 1) for increasing $\lambda$. As discussed above for the CGL case, as $\lambda$ is increased from 2 to 10 from Fig. 6 to Fig. 7, the stabilization due to compressibility is seen first at low $q_D$. Then, as $\lambda$ is further increased to 25 in Fig. 8, almost the entire $(q_D, \theta_2)$-space becomes stable, except for a small sliver in the upper right corner.

Fig. 9 shows the stable region of the $(q_D, \theta_2)$-space for the case of isothermal waves ($\alpha = \beta = 0$, $\varepsilon = \gamma = 1$) for r = 2 and $\lambda = 2$. The structure of the stable space is similar to Fig. 3 for the same r and $\lambda$ values, but with CGL polytrope indices. Fig. 10 shows the stable region for mixed waves ($\alpha = 0$, $\beta = \varepsilon = \gamma = 1$) with r = 0.1 and $\lambda = 2$, which is similar to Fig. 2 for the CGL case. In both Figures 9 and 10, note the unstable band for all $q_D$ near $\theta_2 = \frac{\pi}{2}$ where the stabilizing effect of the magnetic field is weak. Also, for

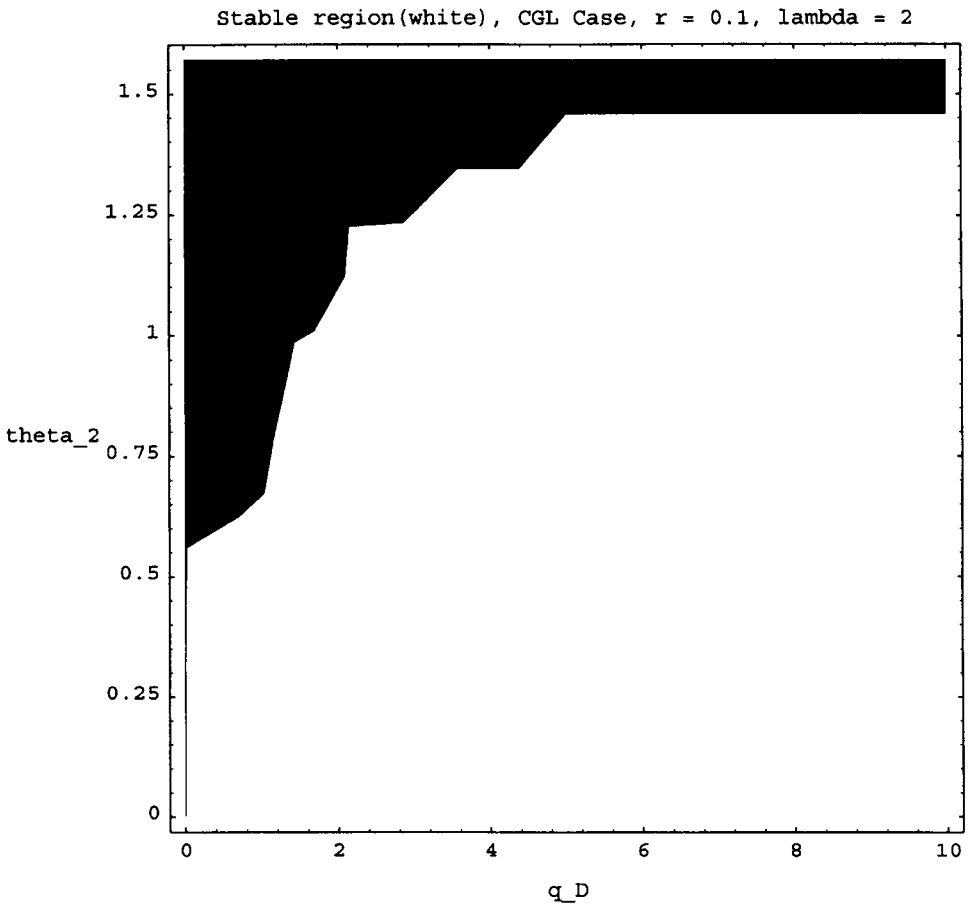


FIG. 2. The stable region (white) in the $(q_D, \theta_2)$-space in the CGL case (polytrope indices $\varepsilon = \beta = 1$, $\alpha = 2$, and $\gamma = 3$) with r = 0.1 and $\lambda = M\cos(\theta_2 - \theta_1) = 2$.

both the isothermal and mixed wave cases, increasing $\lambda$ is found to expand the stable region due to the effect of compressibility discussed earlier. Also, as for the CGL case, the stable region is larger for small r values.

We next consider the special case of modes propagating along the magnetic field in Sec. 4, before considering more general cases in Sec. 5.

**4. Modes with $|W_D| \ll MF$ propagating parallel or antiparallel to the magnetic field.** Now we shall consider the special modes propagating parallel or antiparallel to the magnetic field, so that $\theta_2 = \pm n\pi$ where $n$ is any integer. For $\theta_2 = \pm n\pi$ we have that $T = 0$ and $F = \cos\theta_1$. Thus inequality (14b) becomes

$$\psi_3^2[\psi_1 X^2 + \psi_2(X + \psi_3)] < 0, \tag{15a}$$

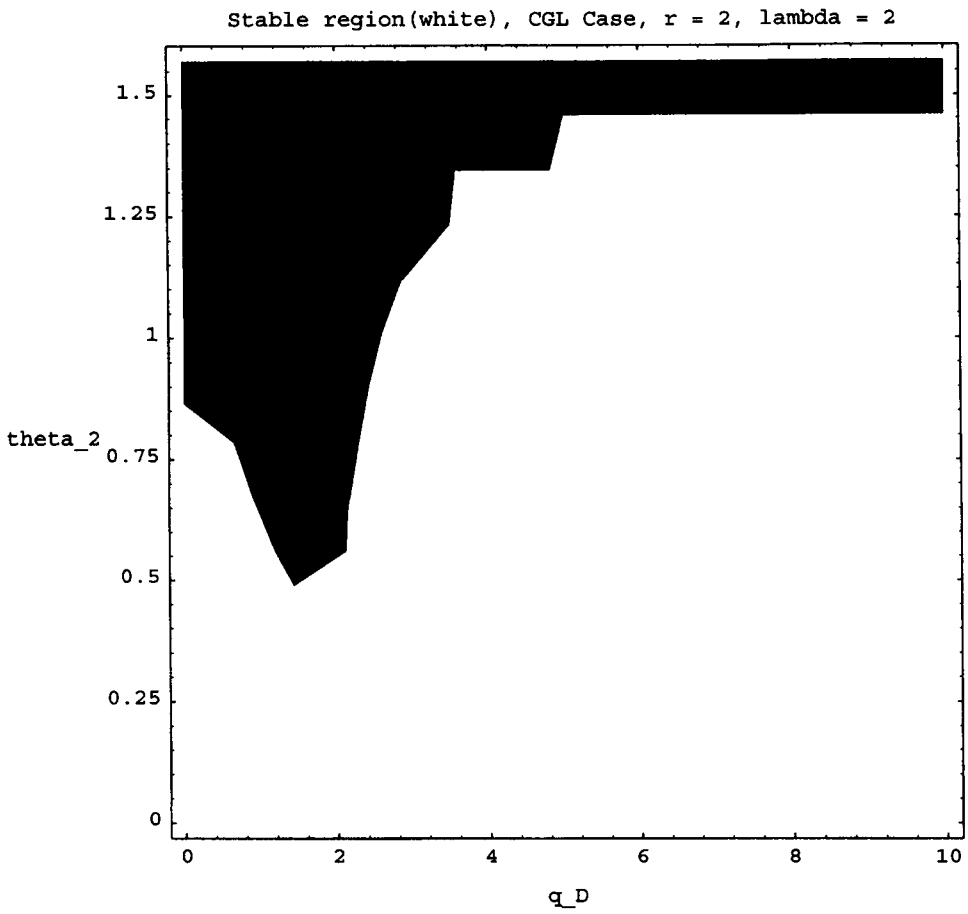


FIG. 3. As in Fig. 2 with r = 2 and $\lambda = 2$.

which may be written as

$$\beta + \varepsilon + q_D^2 < \frac{\varepsilon[(\gamma - 1 - \alpha)\mathrm{r}^2 + 1][\beta + \varepsilon - 1 + (\gamma + 1)\mathrm{r}^2]}{\varepsilon[(\gamma - 1 - \alpha)\mathrm{r}^2 + 1] + [\frac{\mathrm{M}^2 \cos^2\theta_1}{4} - \gamma\mathrm{r}^2]^2}. \tag{15b}$$

Inequality (15b) represents a generalization of inequality (14a) of [34], which is a special case for the CGL indices $\varepsilon = \beta = 1$, $\alpha = 2$, and $\gamma = 3$. Inequality (15a) may be written in the biquadratic form:

$$\frac{\psi_1 \cos^4\theta_1}{16}\mathrm{M}^4 - \frac{\psi_1 \gamma \mathrm{r}^2 \cos^2\theta_1}{2}\mathrm{M}^2 + [\psi_2(1 - \mathrm{r}^2 + q_D^2 - \gamma\mathrm{r}^2) + \psi_1\gamma^2\mathrm{r}^4] < 0. \tag{15c}$$

Noticing that the constant term of (15c) is always positive and examining the discriminant of the expression on the left-hand side of (15c), we find that it is negative and inequalities (15) cannot be satisfied for any value of $\theta_1$ (and $\theta_2 = \pm n\pi$) if

$$\psi_1\gamma^2\mathrm{r}^4(\cos^2\theta_1 - 1) - \psi_2(1 - \mathrm{r}^2 + q_D^2 - \gamma\mathrm{r}^2) < 0. \tag{16}$$

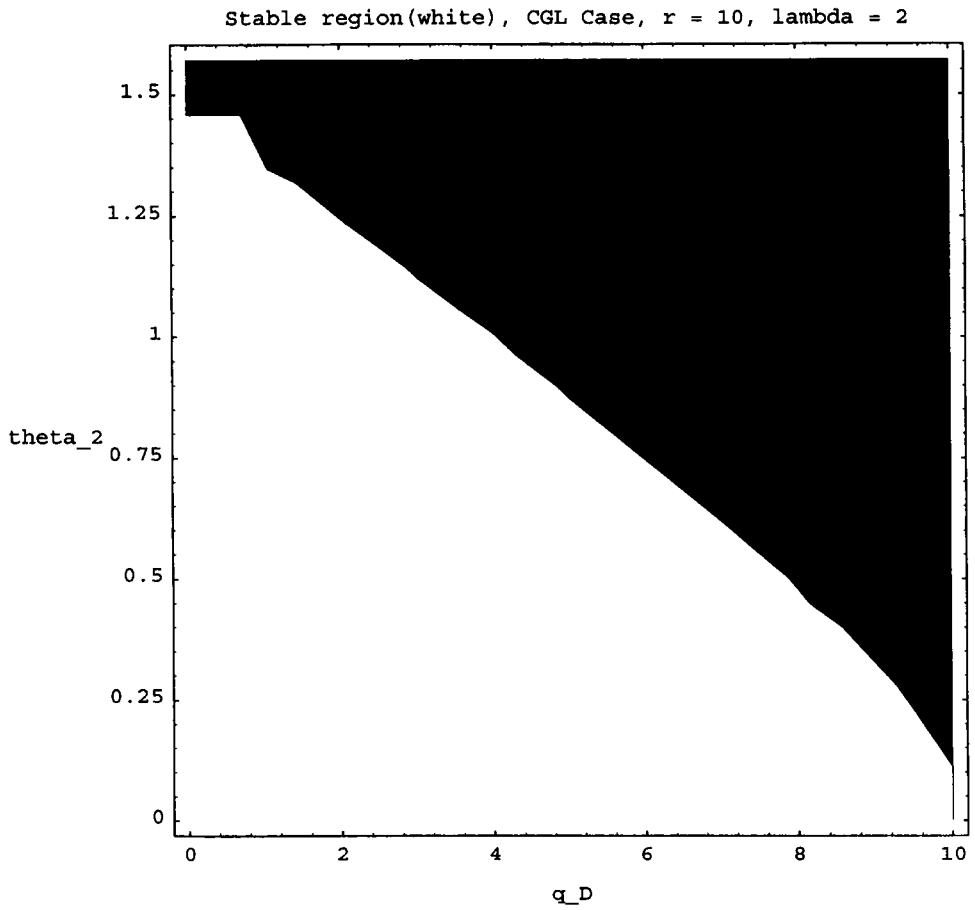


FIG. 4. As in Fig. 2 with r = 10 and $\lambda = 2$.

Using the MHD values of the polytrope indices, $\alpha = 0$, $\beta = 0$, $\varepsilon = \frac{5}{3}$, $\gamma = \frac{5}{3}$, and r = 1, and noticing that $\mathrm{M}_A = \frac{\mathrm{M}}{\mathrm{q}}$ and $q_D^2 = \varepsilon \mathrm{q}^2$, inequality (16) reduces to inequality (23a) of [34]. Also, at

$$\psi_1 \gamma^2 \mathrm{r}^4 (\cos^2 \theta_1 - 1) - \psi_2 (1 - \mathrm{r}^2 + q_D^2 - \gamma \mathrm{r}^2) = 0,$$

both solutions for $M$ coalesce to the value

$$\mathrm{M} = \left( \frac{4\gamma \mathrm{r}^2}{\cos^2 \theta_1} \right)^{\frac{1}{2}} \quad \text{or} \quad \mathrm{M} \cos \theta_1 = 2\mathrm{r}\sqrt{\gamma}.$$

Therefore, we have the significant result that for $\theta_2 = \pm n\pi$, *i.e., for modes propagating along or opposite to the magnetic field direction, no unstable standing wave solutions exist for vortex sheets with*

$$q_D^2 > \frac{\psi_1 \gamma^2 r^4 (\cos^2 \theta_1 - 1)}{\psi_2} - 1 + r^2 - \gamma r^2,$$

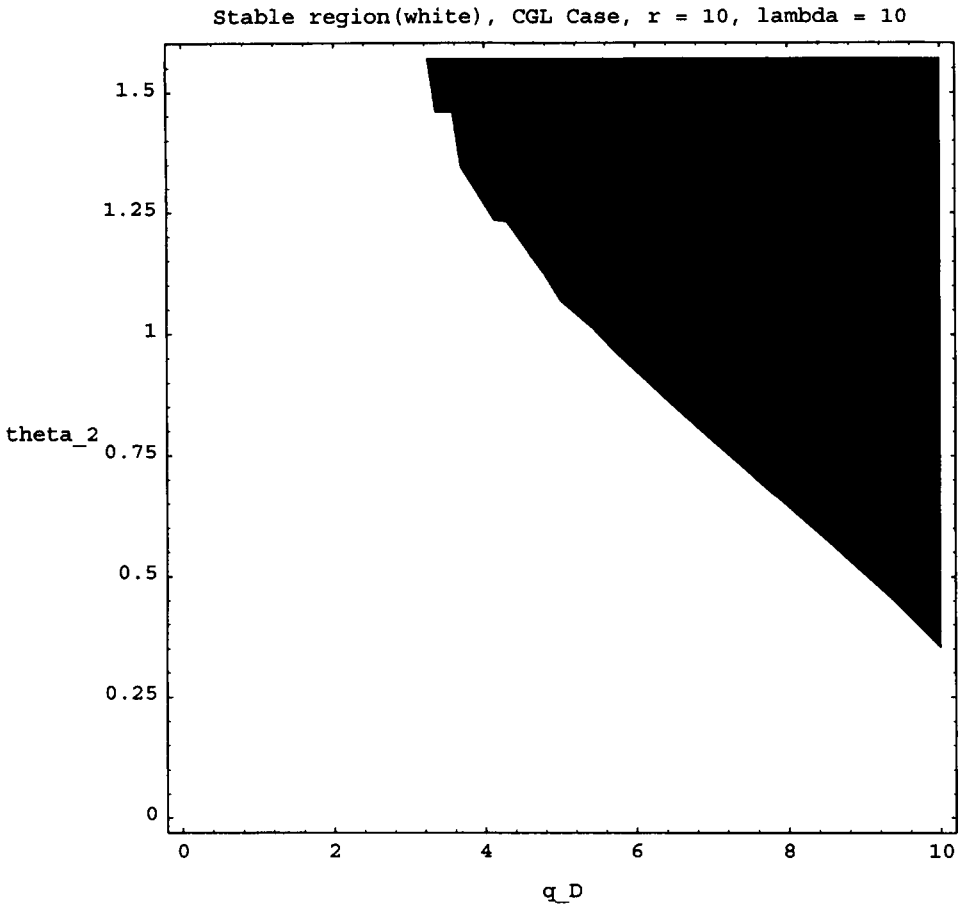


FIG. 5. As in Fig. 2 with r = 10 and $\lambda = 10$.

*for any angle $\theta_1$ of propagation of the flow velocity to the magnetic field.* For the MHD indices $\alpha = \beta = 0$, $\varepsilon = \gamma = \frac{5}{3}$ and r = 1 (for the isotropic, collision-dominated flow), this implies that the modes propagating along or opposite to the magnetic field, and at a general angle to the flow, do not exhibit standing wave instability for the plasma beta $\leq 1$.

**5. Results for arbitrary $\theta_1$ and $\theta_2$.** More generally, for arbitrary values of $\theta_1$ and $\theta_2$, we solve inequalities (14b) and (14c) numerically. In each case, we verify that $|W_D| \ll$ MF from Eq. (13). The assumed inequality is valid, and Eq. (13) represents a valid solution of Eq. (11), for all the results presented. Specifically, we pick values of $q_D$, r, and T, and solve for the range of X (see Eq. (12c)), and therefore MF, in which inequality (14b) is satisfied. This inequality defines the boundaries of the regime of unstable standing modes in the (MF, $q_D$) plane. Next, we verify that inequality (14c) is satisfied in this range. And, finally we check, from Eq. (13), that the assumed ordering

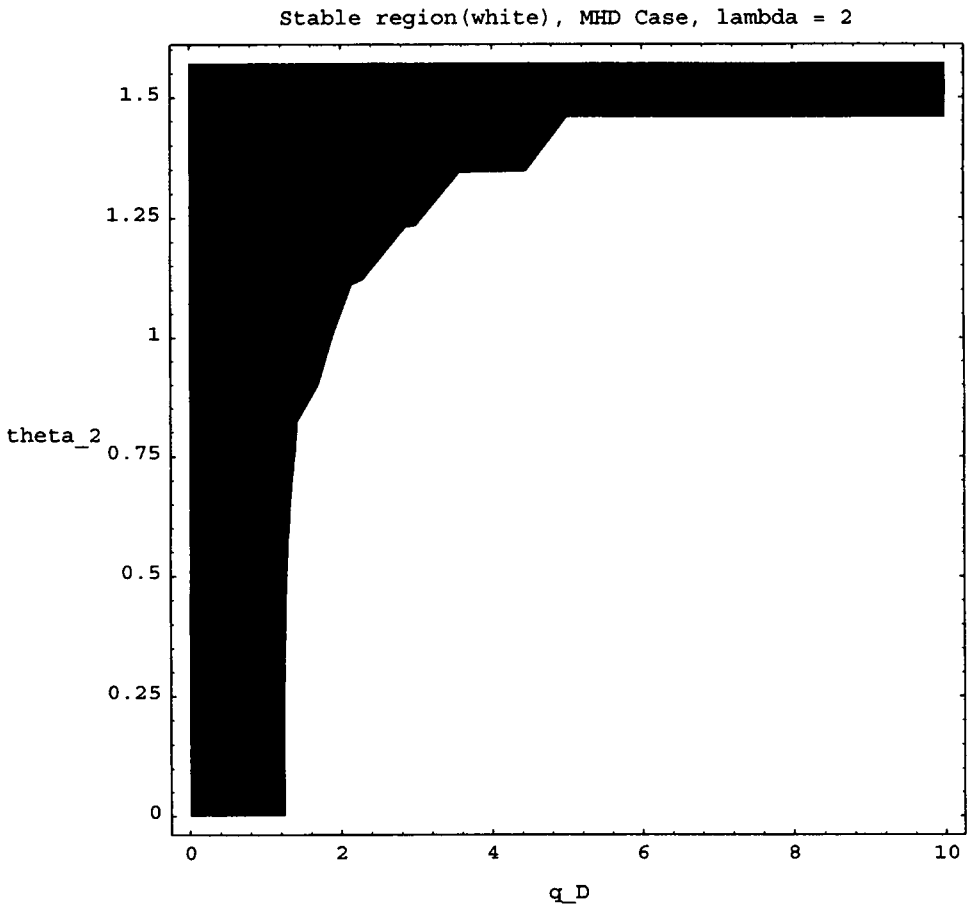


FIG. 6. The stable region (white) in the $(q_D, \theta_2)$-space in the MHD case (polytrope indices $\alpha = \beta = 0$, $\varepsilon = \gamma = \frac{5}{3}$, r = 1) with $\lambda = 2$.

$|W_D| \ll MF$ is valid in this range. In the majority of cases, we pick $\theta_2 \geq \pi/4$ ($T \geq 1$), so that the stabilizing effect of the magnetic field line tension is relatively small, and we are in the more unstable regions of greater interest in physical problems.

In the rest of this section, we first consider CGL modes (polytrope indices $\varepsilon = \beta = 1$, $\alpha = 2$, and $\gamma = 3$), followed by MHD modes (polytrope indices $\alpha = \beta = 0$, $\varepsilon = \gamma = \frac{5}{3}$), isothermal wave modes (polytrope indices $\alpha = \beta = 0$, $\varepsilon = \gamma = 1$), where we use an isothermal equation of state for both pressures (parallel and perpendicular), mixed wave modes (polytrope indices $\alpha = 0$, $\beta = \varepsilon = \gamma = 1$), where the first adiabatic invariant is conserved but an isothermal equation is used for the parallel pressure [29], and finally we shall look at an interesting instability diagram.

Let us consider the CGL case. For this case we have Figures 11 through 15. Fig. 11 shows the unstable standing wave regimes in the $(MF, q_D)$-plane for r = 0.1 and T = 1 ($\theta_2 = 45°$). The upper limiting curve is given by $q_D = \left(r^2 - 1 + \frac{M^2F^2}{4}\right)^{\frac{1}{2}}$ (or, $\psi_3 = 0$, see Eq. (12c)) in this figure since the radicand is positive for all values of MF. The nonzero

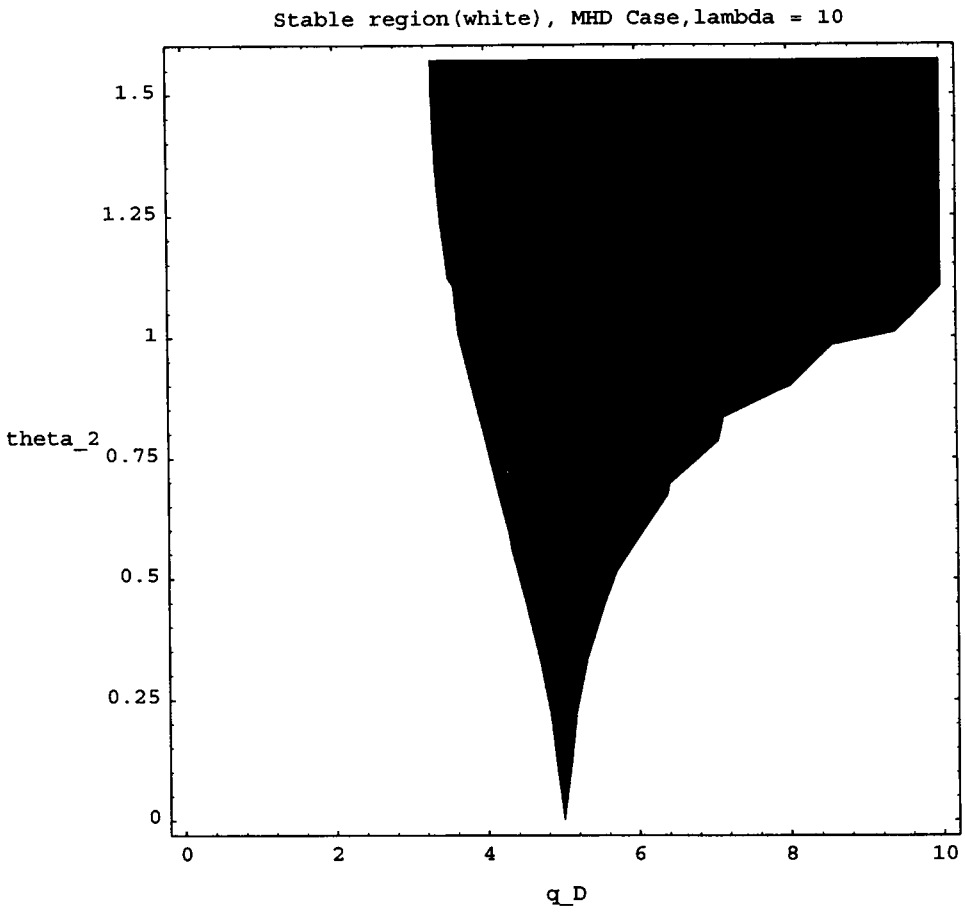


FIG. 7. As in Fig. 6 with $\lambda = 10$.

value of T alters the nature of the standing wave instability considerably. For T = 0, the standing wave instability does not exist for $r < \frac{1}{2}(1+q_D^2)^{\frac{1}{2}}$. Therefore, the standing wave instability would be absent everywhere in the (MF, $q_D$)-plane of Fig. 1 with T = 0.

Fig. 12 shows the unstable standing wave regimes for r = 0.1 and T = 10 ($\theta_2 = 84.29°$). The curve here is given by $q_D = \left(r^2 - 1 + \frac{M^2F^2}{4}\right)^{\frac{1}{2}}$. The regime of standing wave instability has enlarged greatly from that of Fig. 11. There is a lower limiting curve for the regime of instability, from (14b), but it is not present for MF < 40.

Fig. 13 shows the unstable standing wave regimes for r = 2 and T = 0.5 ($\theta_2 = 26.57°$). The smooth upper limiting curve is again given by $q_D = \left(r^2 - 1 + \frac{M^2F^2}{4}\right)^{\frac{1}{2}}$. The lower limiting curve comes from the other factor of Eq. (14b) which is quadratic in MF. Notice that the curves only cover MF $\geq 1$. This is to indicate that the assumed $|W_D| \ll$ MF ordering, used in deriving Eq. (14b), is valid in this range. This case is the same as that

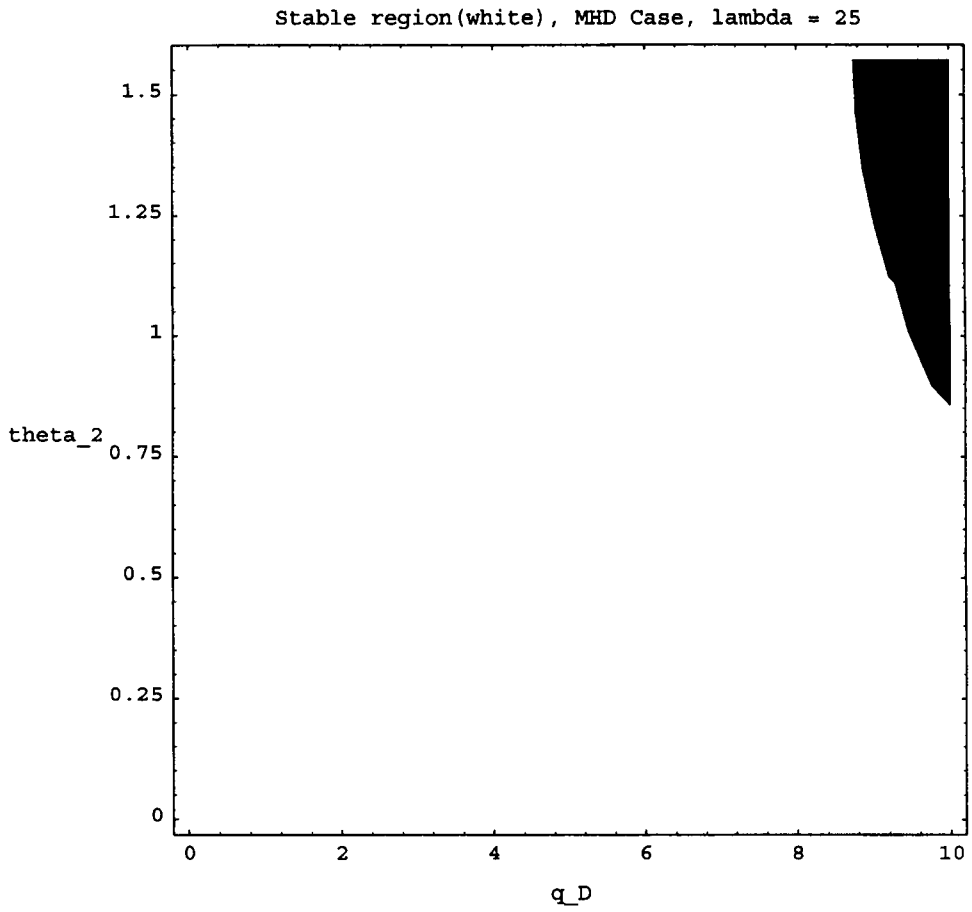


FIG. 8. As in Fig. 6 with $\lambda = 25$.

of Fig. 3 in [34]. When comparing Fig. 13 to Fig. 3 of [34], please note that the axes have been inverted.

Fig. 14 shows the unstable standing wave regimes for r = 2 and T = 10 ($\theta_2 = 84.29°$). This figure is similar to Fig. 12, with the exception that the anisotropy parameter, r, has been increased from 0.1 to 2. This has the effect of inverting the curve given by $q_D = \left(r^2 - 1 + \frac{M^2F^2}{4}\right)^{\frac{1}{2}}$. Again, there is a lower limiting curve, from (14b), that exists for MF $\geq 40$.

Fig. 15 shows the unstable standing wave regimes for r = 10 and T = 0.5 ($\theta_2 = 26.57°$). Here, the anisotropy parameter, r, has been increased to r = 10. We can see that the region of instability, when compared to Fig. 13 (where T = 0), has been increased. The region of instability has also been shifted to higher values of $q_D$.

The criterion for unstable traveling wave modes is Eq. (14c) with the inequality reversed. For $\theta_1 = \theta_2 = 0$ [20], inequality (14c) is always satisfied and no traveling modes

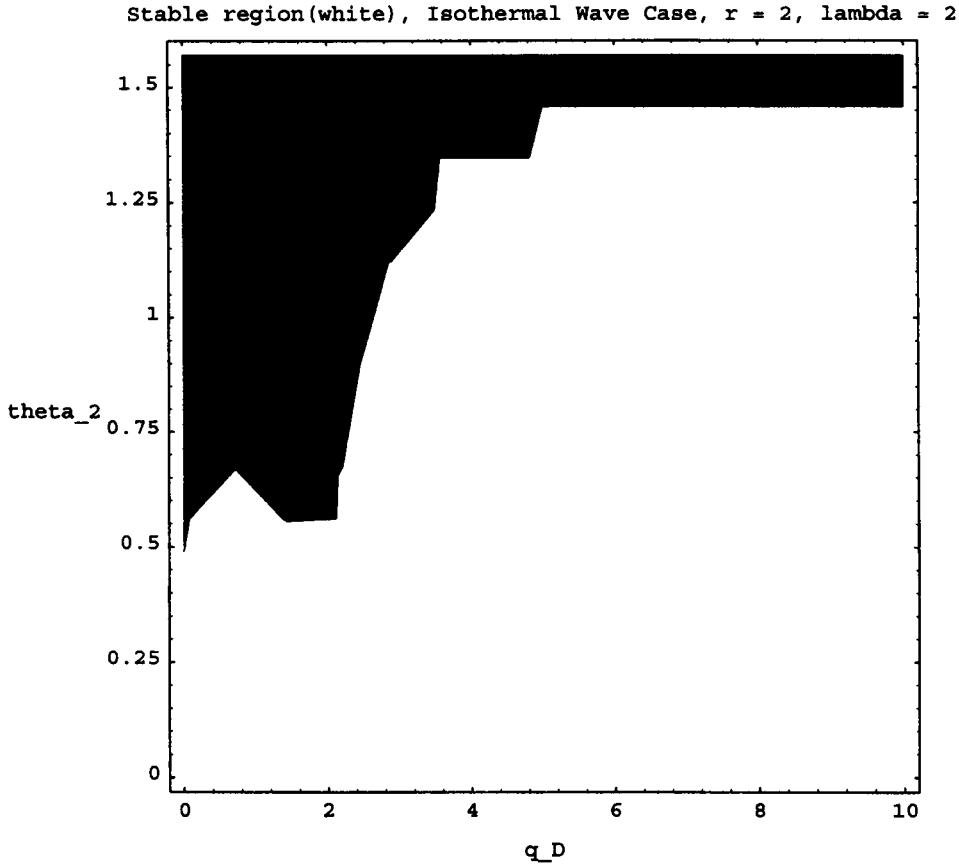


FIG. 9. The stable region (white) in the $(q_D, \theta_2)$-space for the isothermal wave case (polytrope indices $\alpha = \beta = 0$, $\varepsilon = \gamma = 1$) with r = 2 and $\lambda = 2$.

satisfying the ordering $|W_D| \ll$ MF exist. Similarly, in all the cases considered numerically here, inequality (14c) is always satisfied and traveling modes with the assumed ordering for $|W_D|$ and MF are absent. It appears that the $|W_D| \ll$ MF solutions automatically exclude the traveling modes. This is borne out by the general analytical solutions for T = 0 in Sec. 6 without the assumption $|W_D| \ll$ MF, where it is explicitly found that the traveling modes violate the ordering $|W_D| \ll$ MF, while the standing modes satisfy it.

Next, let us consider the MHD case. For this case we have Figures 16 and 17. Fig. 16 shows the unstable standing wave regimes for r = 1 and T = 1 ($\theta_2 = 45°$). Again, when comparing these figures to those of [34], note that the axes are inverted, and also note that $M_A = \frac{M}{q}$ and $q_D^2 = \varepsilon q^2$, as mentioned in Sec. 4. For the collision-dominated MHD case, the pressure is isotropic and r = 1. Here, we have large regions of stability with the unstable region being confined to values of $q_D$ that are slightly less than $\frac{MF}{2}$. This figure has a similar shape to that of Fig. 11 (CGL case) for the same value of T.

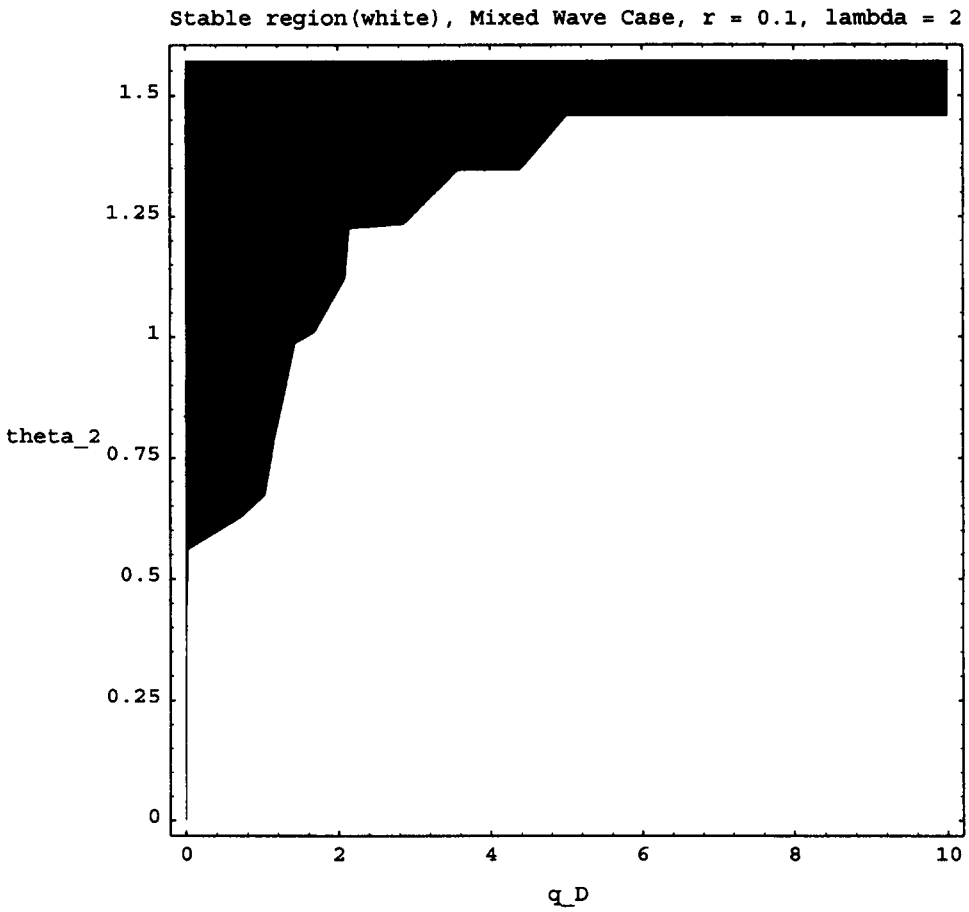


FIG. 10. The stable region (white) in the $(q_D, \theta_2)$-space in the mixed wave case (polytrope indices $\alpha = 0$, $\beta = \varepsilon = \gamma = 1$) with r = 0.1 and $\lambda = 2$.

Fig. 17 shows the unstable standing wave regimes for T = 10 ($\theta_2 = 84.29°$). We see that increasing the value of T from 1 to 10 has enlarged the region of instability from that of Fig. 16. As for the CGL case, the criterion for unstable traveling wave modes, Eq. (14c) with the inequality reversed, is never satisfied and thus no traveling modes satisfying $|W_D| \ll MF$ exist.

Figures 18 through 20 correspond to isothermal wave cases. Fig. 18 shows the unstable standing wave regimes in the $(MF, q_D)$-plane for r = 0.1 and T = 10 ($\theta_2 = 84.29°$). The upper limiting curve is again given by $q_D = \left(r^2 - 1 + \frac{M^2F^2}{4}\right)^{\frac{1}{2}}$ (or, $\psi_3 = 0$, see Eq. (12c)). The region of instability here is similar to that of Fig. 11 (for the CGL case with the same $r$ value), noting that the lower limiting curve has moved to larger values of MF thus increasing the region of instability. The behavior of the two systems is virtually the same. Note that this is certainly not obvious *a priori* since the polytrope indices for the two cases are very different.

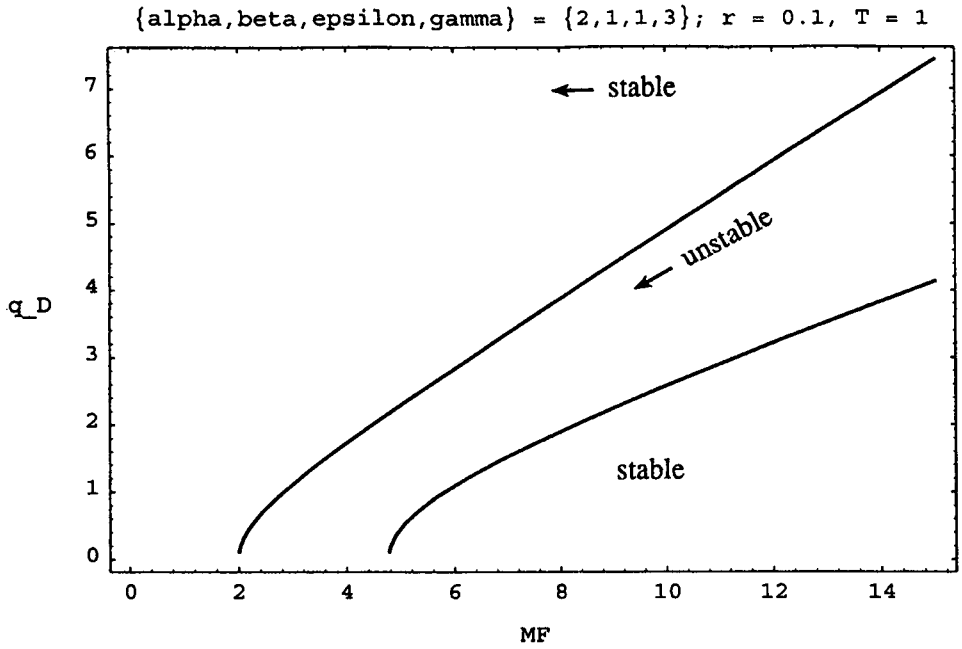


FIG. 11. The unstable standing wave regimes in the $(\mathrm{MF}, \mathrm{q_D})$-plane for r = 0.1 and T = 1 ($\theta_2 = 45°$), for the CGL wave case (polytrope indices $\varepsilon = \beta = 1$, $\alpha = 2$, and $\gamma = 3$). In the intermediate region, the vortex sheet is unstable and the growth rate is given by Eq. (13) for all values of MF. The upper limiting curve is given by $\mathrm{q_D} = \left(\mathrm{r}^2 - 1 + \frac{\mathrm{M}^2\mathrm{F}^2}{4}\right)^{\frac{1}{2}}$ (or, $\psi_3 = 0$, see Eq. (12c)).

Fig. 19 is similar to Fig. 18. The value of r has been increased from 0.1 to 10 and this has had the effect of inverting the upper limiting curve. However, the region of instability in both figures has the same shape and equivalent size.

Fig. 20 shows the unstable standing wave regimes in the $(\mathrm{MF}, q_D)$-plane for r = 10 and T = 2 ($\theta_2 = 63.43°$). This figure is similar in shape to Fig. 13 (CGL case); the region of instability has a branch that extends downward to $q_D = 0$. However, here the region of instability is wider and seems to be opening up as MF increases, whereas in Fig. 13, the boundaries appear to be remaining a fixed distance apart. It seems that an increase in the anisotropy parameter, r, has the effect of enlarging the region of instability and shifting it to higher values of $q_D$.

Figures 21 and 22 correspond to the mixed wave case. Fig. 21, with r = 0.1 and T = 10 ($\theta_2 = 84.29°$), is again similar to Fig. 17 (MHD case) as well as Figures 18 and 19 (isothermal case). Fig. 22, with r = 2 and T = 5 ($\theta_2 = 78.69°$), has a similar shape as Fig. 19 (isothermal case) with the upper limiting curve being inverted. The value of r is the same as in Fig. 18 which accounts for the similarity of shape.

Fig. 23 is an interesting instability diagram. It has polytrope indices $\alpha = \beta = \varepsilon = \gamma = 1$, with r = 2, and T = 0.5 ($\theta_2 = 26.57°$). Inequality (14b) has three factors, $\psi_3$ and two factors from the long curly bracket. The parabolic region of instability and the

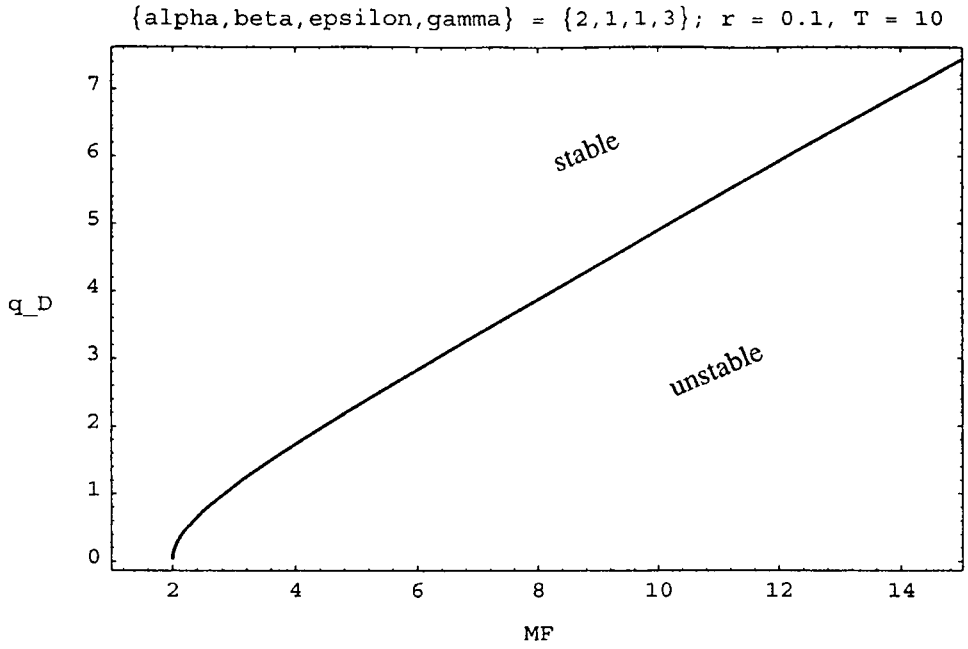


FIG. 12. As in Fig. 11 with r = 0.1 and T = 10 ($\theta_2 = 84.29°$).

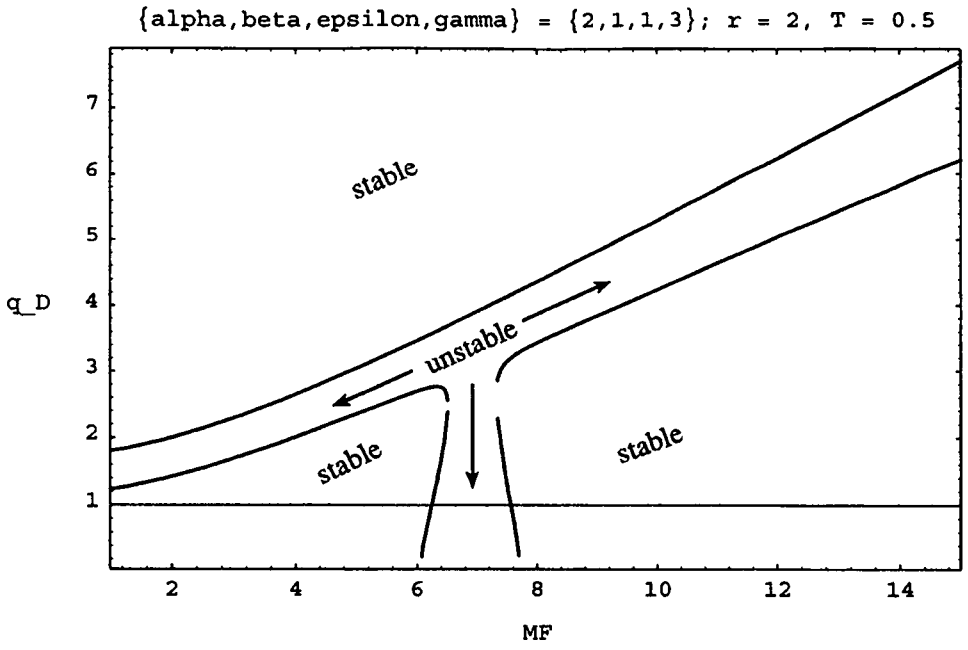


FIG. 13. As in Fig. 11 with r = 2 and T = 0.5 ($\theta_2 = 26.57°$).

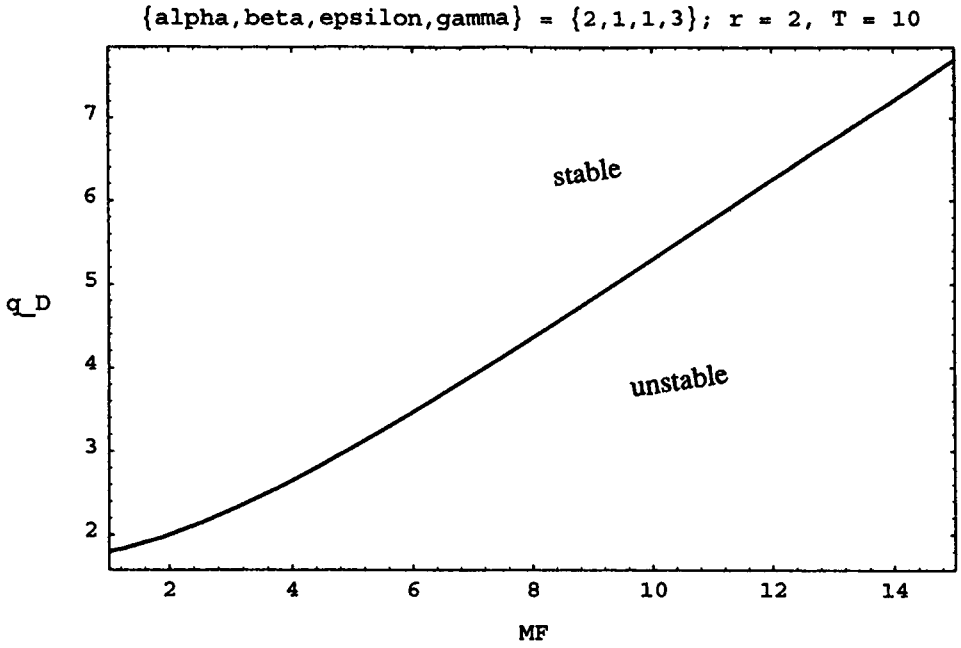


FIG. 14. As in Fig. 11 with r = 2 and T = 10 ($\theta_2 = 84.29°$).

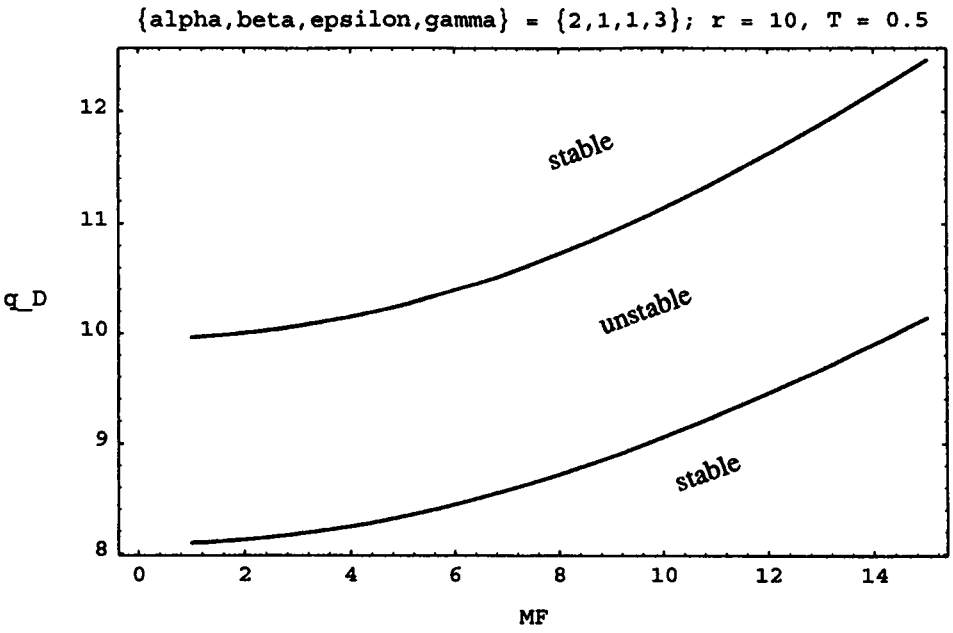


FIG. 15. As in Fig. 11 with r = 10 and T = 0.5 ($\theta_2 = 26.57°$).

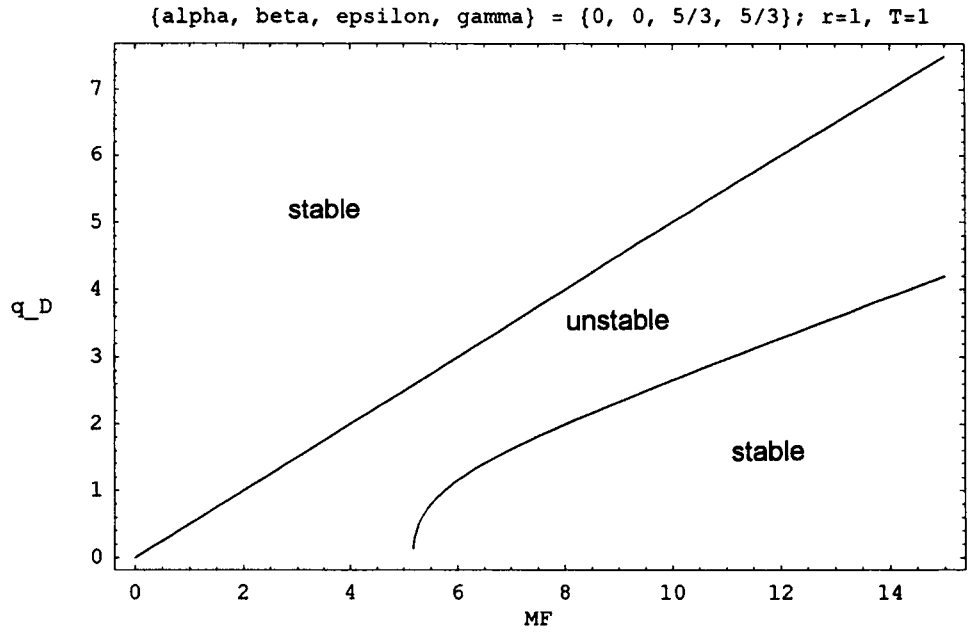


FIG. 16. The unstable standing wave regimes in the $(\mathrm{MF}, q_D)$-plane for r = 1 and T = 1 ($\theta_2 = 45°$), for the MHD wave case (polytrope indices $\alpha = \beta = 0$, $\varepsilon = \gamma = \frac{5}{3}$). In the intermediate region, the vortex sheet is unstable and the growth rate is given by Eq. (13) for all values of MF.

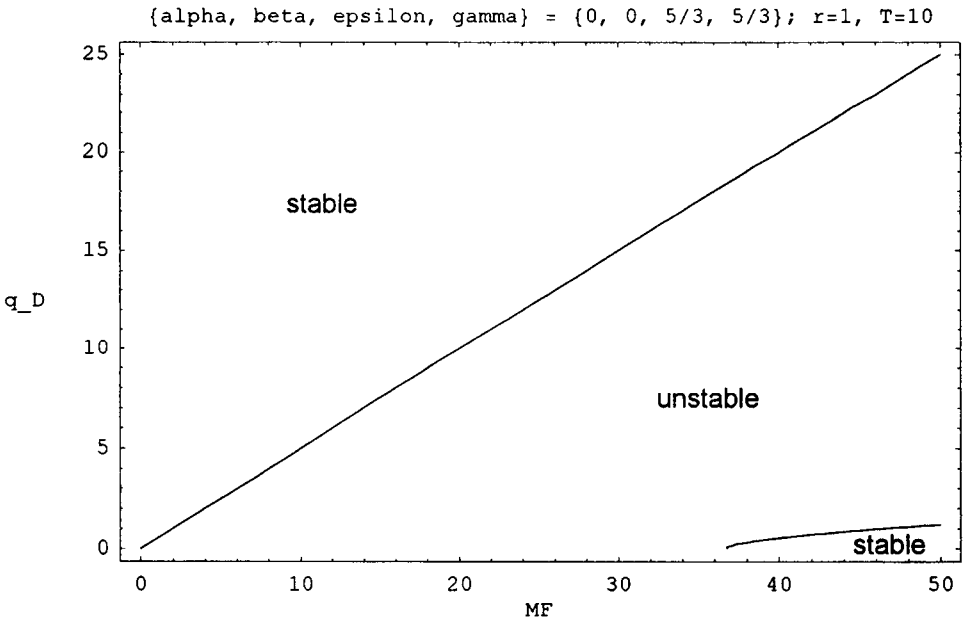


FIG. 17. As in Fig. 16 with r = 1 and T = 10 ($\theta_2 = 84.29°$).

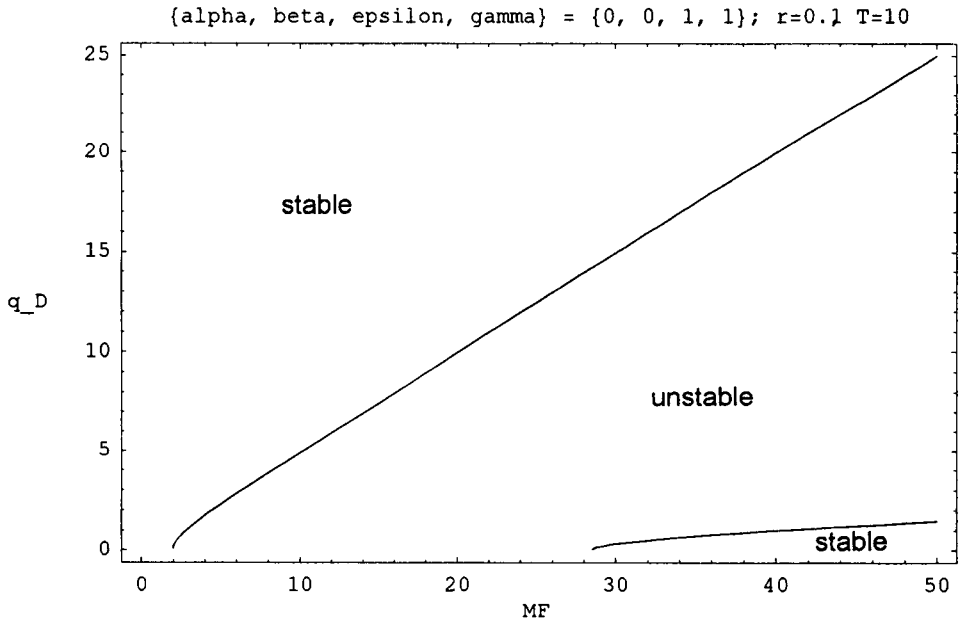


FIG. 18. The unstable standing wave regimes in the $(\mathrm{MF}, q_D)$-plane for r = 0.1 and T = 10 ($\theta_2 = 84.29°$), for the isothermal wave case (polytrope indices $\alpha = \beta = 0$, $\varepsilon = \gamma = 1$). In the intermediate region, the vortex sheet is unstable and the growth rate is given by Eq. (13) for all values of MF. The upper limiting curve is given by $q_D = \left(r^2 - 1 + \frac{M^2F^2}{4}\right)^{\frac{1}{2}}$ (or, $\psi_3 = 0$, see Eq. (12c)).

lower limiting curve (with a cusp at MF $\approx 4.2$) come from the quadratic factor in the curly bracket of Eq. (14b) and the smooth (almost linear) curve comes from $\psi_3$. Figures 13 and 19 have corresponding values of r and T; however, the change in the polytrope indices has produced a rather dramatic shift in the region of standing wave instability.

**6. General instability criteria for $\theta_2 = 0$ and arbitrary $|W_D|$.** In this section, we consider the special case $\theta_2 = 0$ when the general dispersion (11) relation is biquadratic. Thus, we shall be able to derive the conditions for both standing wave and traveling wave modes without making the assumption $|W_D| \ll$ MF of Sec. 3. We shall prove thereby that (14b), derived under the assumption $|W_D| \ll$ MF, represents the general criterion for standing wave instability.

For $\theta_2 = 0$ we have that T = 0 and thus the general dispersion relation (11) becomes

$$\frac{[\psi_1(X - MW_D + W_D^2) + \psi_2][\psi_3 + MW_D - W_D^2]}{(X - MW_D + W_D^2)} = \frac{[\psi_1(X + MW_D + W_D^2) + \psi_2][\psi_3 - MW_D - W_D^2]}{(X + MW_D + W_D^2)}. \tag{17a}$$

After cross-multiplying, we get

$$2M\psi_1 W_D^5 + (4M\psi_1 X - 2M^3\psi_1)W_D^3 + (2M\psi_2\psi_3 + 2M\psi_2 X + 2M\psi_1 X^2)W = 0, \tag{17b}$$

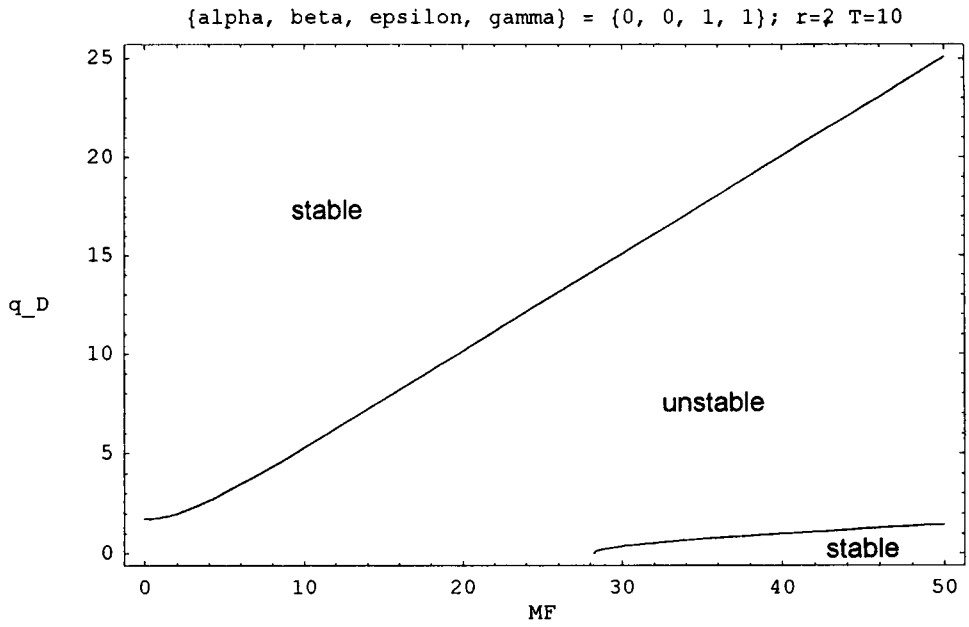


FIG. 19. As in Fig. 18 with r = 2 and T = 10 ($\theta_2 = 84.29°$).

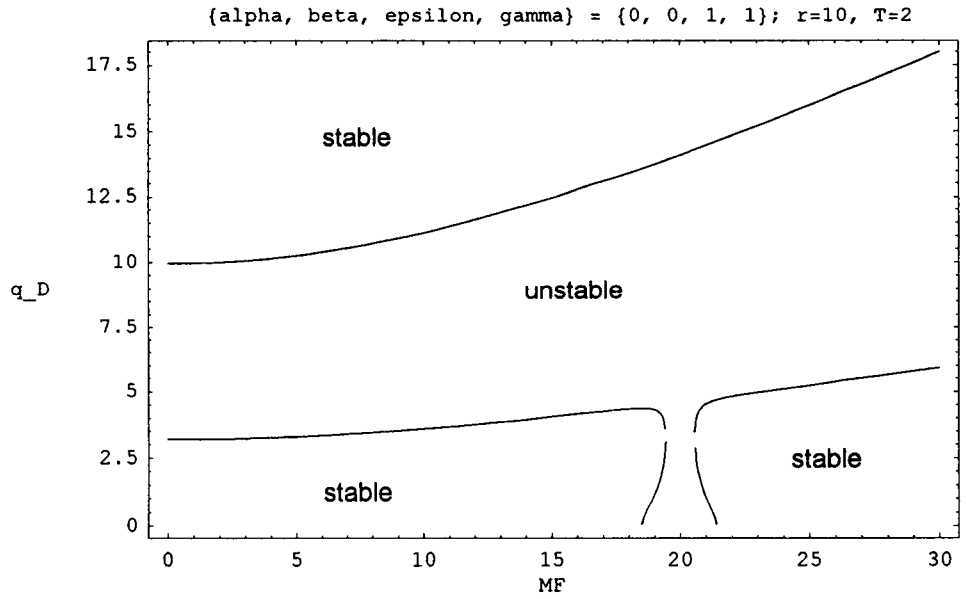


FIG. 20. As in Fig. 18 with r = 10 and T = 2 ($\theta_2 = 63.43°$).

and dividing by $(2MW_D)$ results in

$$c_5 W_D^4 + c_3 W_D^2 + c_1 = 0 \tag{17c}$$

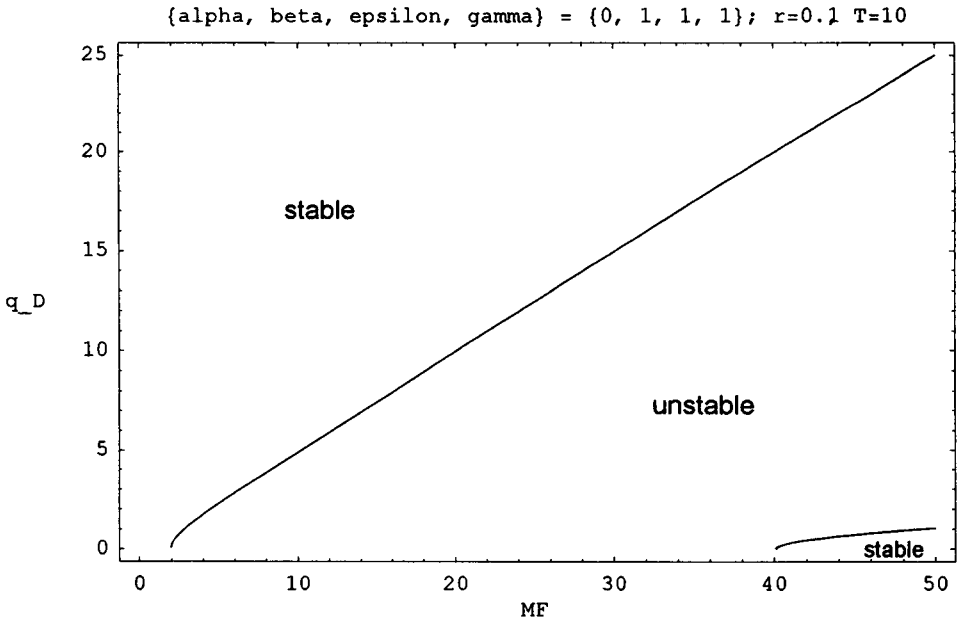


FIG. 21. The unstable standing wave regimes in the $(\mathrm{MF}, q_D)$-plane for r = 0.1 and T = 10 ($\theta_2 = 84.29°$), for the mixed wave case (polytrope indices $\alpha = 0$, $\beta = \varepsilon = \gamma = 1$). In the intermediate region, the vortex sheet is unstable and the growth rate is given by Eq. (13) for all values of MF.

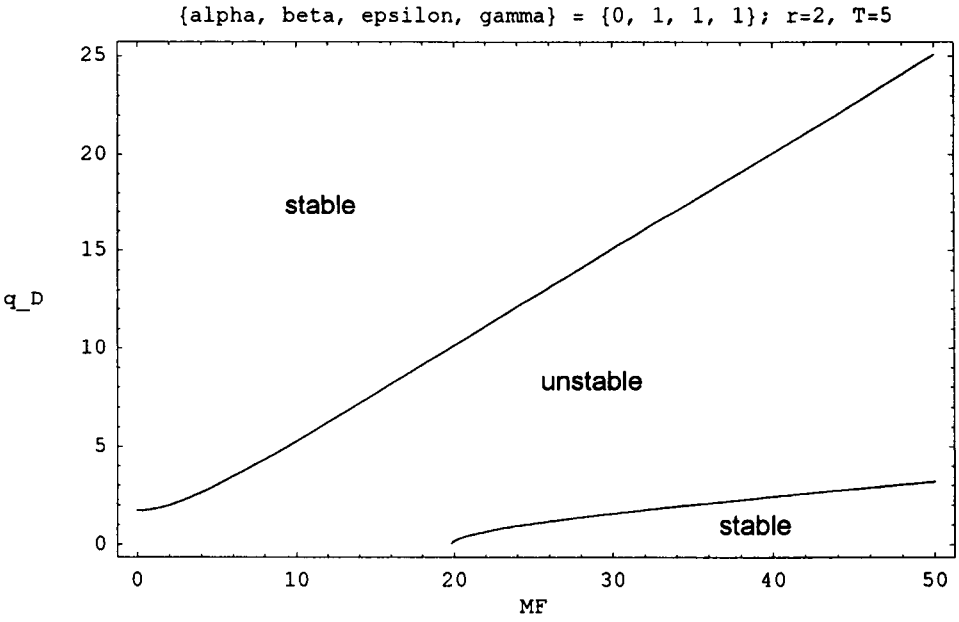


FIG. 22. As in Fig. 21 with r = 2 and T = 5 ($\theta_2 = 78.69°$).

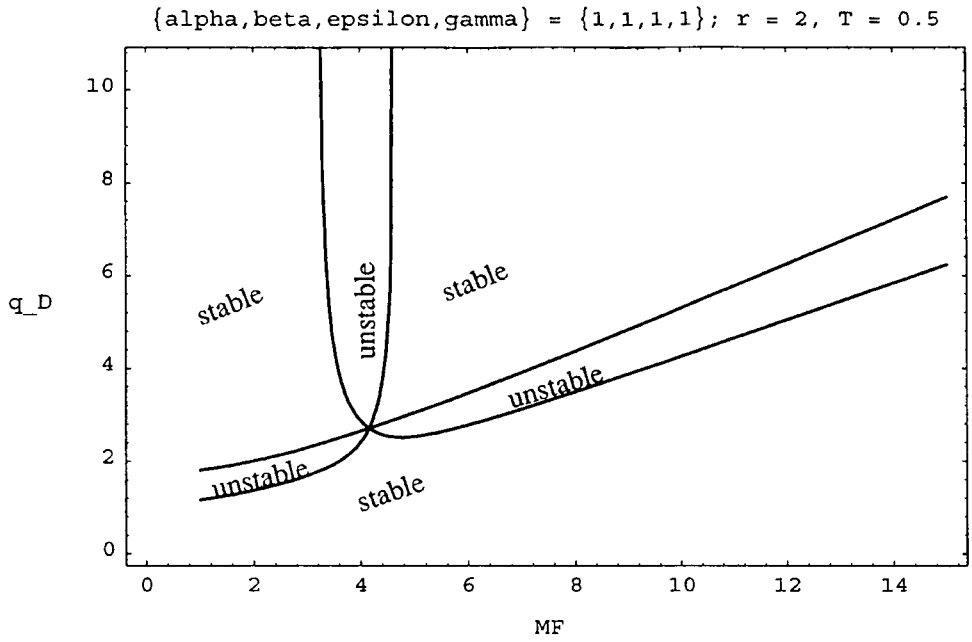


FIG. 23. The unstable standing wave regimes in the $(\mathrm{MF}, q_D)$-plane for r = 2 and T = 0.5 ($\theta_2 = 26.57°$), for the interesting instability diagram (polytrope indices $\alpha = \beta = \varepsilon = \gamma = 1$). In the intermediate region, the vortex sheet is unstable and the growth rate is given by Eq. (13) for all values of MF.

which is biquadratic, with

$$\begin{aligned} c_5 &= \psi_1, \\ c_3 &= 2\psi_1 X - M^2\psi_1, \\ c_1 &= \psi_1 X^2 + \psi_2(X + \psi_3). \end{aligned} \tag{18}$$

Similar to the argument in Sec. 3, we have that the condition for standing wave instability, $W_D$ pure imaginary, is

$$c_1 < 0, \tag{19a}$$

which may be written as

$$\psi_1 X^2 + \psi_2(X + \psi_3) < 0. \tag{19b}$$

Now, inequality (14b) with T = 0 reduces exactly to inequality (19b). Thus criterion (14b), which was derived under the assumption $|W_D| \ll \mathrm{MF}$, actually recovers the general criterion for standing wave instability without making this assumption. This is because the standing wave modes satisfy the assumption $|W_D| \ll \mathrm{MF}$, as may be checked *a posteriori* for the general values of $\theta_2$ in the examples considered in Sec. 5. On the contrary, the traveling wave solutions violate the approximation $|W_D| \ll \mathrm{MF}$, and are thus omitted when the general quartic dispersion relation (11) is reduced to the quadratic equation (12a) via this assumption. As mentioned in Sec. 5, this also shows up in the

criterion $b_3^2 < 4b_1b_5$ (criterion (14c) reversed) for traveling wave modes in Eq. (13) never being satisfied in our numerical investigations.

## References


[1] A. K. Sen, *Stability of the magnetosphere boundary*, Planetary and Space Science **13**, 131–141 (1965)

[2] J. F. Mckenzie, *Hydromagnetic oscillations of the geomagnetic tail and plasma sheet*, J. Geophysical Res. **75**, 5331–5339 (1970)

[3] D. J. Southwood, *Some features of the field line resonances in the magnetosphere*, Planetary and Space Science **22**, 483–491 (1974)

[4] L. Chen and A. Hasegawa, *A theory of long-period magnetic pulsations*, J. Geophysical Res. **79**, 1024–1032 (1974)

[5] F. L. Scarf, W. S. Kurth, D. A. Gurnett, H. S. Bridge, and J. D. Sullivan, *Jupiter tail phenomena upstream from Saturn*, Nature **292**, 585–586 (1981)

[6] H. Dobrowolny and N. D'Angelo, *Wave motion in type I comet tails*, in *Cosmic Plasma Physics* (K. Schindler, ed.), Plenum, New York, 1972

[7] A. I. Ershkovich, A. A. Nusnov, and A. A. Chernikov, *Oscillations of type I comet tails*, Planetary and Space Science **20**, 1235–1243 (1972); and, *Nonlinear waves in type I comet tails*, **21**, 663–673 (1973)

[8] B. D. Turland and P. A. G. Scheuer, *Instabilities of Kelvin-Helmholtz type for relativistic streaming*, Monthly Notices Roy. Astron. Soc. **176**, 421–441 (1976)

[9] R. D. Blandford and J. E. Pringle, *Kelvin-Helmholtz instability of relativistic beams*, Monthly Notices Roy. Astron. Soc. **176**, 443–454 (1976)

[10] S. Chandrasekhar, *Hydrodynamic and Hydromagnetic Stability*, Dover (originally published 1961, Oxford, Clarendon), New York, 1981; A. Syrovatskii, *The Helmholtz instability*, Soviet Physics Uspekhi **62**, 247–253 (1957); T. G. Northrop, *Helmholtz instability of a plasma*, Physical Review (Second series) **103**, 1150–1154 (1956)

[11] R. A. Gerwin, *Stability of the interface between two fluids in relative motion*, Rev. Modern Phys. **40**, 652–658 (1968)

[12] T. P. Ray and A. I. Ershkovich, *Kelvin-Helmholtz instabilities of magnetized shear layers*, Monthly Notices Roy. Astron. Soc. **204**, 821–826 (1983)

[13] A. Miura, *Anomalous transport by magnetohydrodynamic Kelvin-Helmholtz instabilities in the solar wind-magnetosphere interaction*, J. Geophysical Res. **89**, 801–818 (1984)

[14] S. Roy Choudhury and R. V. Lovelace, *On the Kelvin-Helmholtz instabilities of supersonic shear layers*, Astrophysical J. **283**, 331–342 (1984); and, *On the Kelvin-Helmholtz instabilities of high-velocity magnetized shear layers* **302**, 188–199 (1986); A. Miura and P. L. Pritchett, *Nonlinear stability analysis of the MHD Kelvin-Helmholtz instability in a compressible plasma*, J. Geophysical Res. **87**, 7431–7444 (1982)

[15] S. Roy Choudhury, *Kelvin-Helmholtz instabilities of supersonic, magnetized shear layers*, J. Plasma Phys. **35**, 375–392 (1986)

[16] C. Uberoi, *On the Kelvin-Helmholtz instabilities of structured plasma layers in the magnetosphere*, Planetary and Space Science **34**, 1223–1227 (1986)

[17] M. Fujimota and T. Terasawa, *Ion inertia effect on the Kelvin-Helmholtz instability*, J. Geophysical Res. **96**, 15725–15734 (1991)

[18] A. C. Sharma and K. M. Shrivastava, *Magnetospheric plasma waves*, Astrophys. Space Sci. **200**, 107–115 (1993)

[19] S. K. Malik and M. Singh, *Chaos in Kelvin-Helmholtz instability in magnetic fluids*, Phys. Fluids A **4**, 2915–2922 (1992)

[20] S. Roy Choudhury and V. L. Patel, *Kelvin-Helmholtz instabilities of high-velocity, magnetized anisotropic shear layers*, Phys. Fluids **28**, 3292–3301 (1985)

[21] S. Duhau, F. Gratton, and J. Gratton, *Hydromagnetic oscillations of a tangential discontinuity in the CGL approximation*, Phys. Fluids **13**, 1503–1509 (1970)

[22] S. Duhau, F. Gratton, and J. Gratton, *Radiation of hydromagnetic waves from a tangential velocity discontinuity*, Phys. Fluids **14**, 2067–2071 (1971)

[23] S. Duhau and J. Gratton, *Effect of compressibility on the stability of a vortex sheet in an ideal magnetofluid*, Phys. Fluids **16**, 150–152 (1972)

[24] R. Rajaram, G. L. Kalra, and J. N. Tandon, *Discontinuities and the magnetospheric phenomena*, J. Atm. Terr. Phys. **40**, 991–1000 (1978)
[25] R. Rajaram, G. L. Kalra, and J. N. Tandon, *Discontinuities in the magnetosphere*, Astrophys. Space Sci. **67**, 137–150 (1980)
[26] S. P. Talwar, *Hydromagnetic stability of the magnetospheric boundary*, J. Geophysical Res. **69**, 2707–2713 (1964)
[27] S. P. Talwar, *Kelvin-Helmholtz instability in an anisotropic plasma*, Phys. Fluids **8**, 1295–1299 (1965)
[28] Zu-Yin Pu, *Kelvin-Helmholtz instability in collisionless space plasmas*, Phys. Fluids B **1**, 440–447 (1989)
[29] B. A. Shrauner, *Small amplitude hydromagnetic waves for a plasma with a generalized polytrope law*, Plasma Phys. **15**, 375–385 (1973)
[30] G. Mattei, Accademia Nazionale Dei Lincei Lxiv, 170 (1978)
[31] D. Summers, *Polytropic solutions to the problem of spherically symmetric flow of an ideal gas*, Canadian J. of Phys. **58**, 1085–1092 (1980)
[32] M. Dobróka, *Coupled waves in stratified plasmas, treated by generalized polytropic equation of state*, Plasma Phys. **24**, 1401–1410 (1982)
[33] K. G. Brown and S. Roy Choudhury, *Kelvin-Helmholtz instabilities of high velocity magnetized shear layers with generalized polytrope laws*, Quarterly of Applied Math. **58**, 401–423 (2000)
[34] S. Roy Choudhury, *An analytical study of the Kelvin-Helmholtz instabilities of compressible, magnetized anisotropic tangential velocity discontinuities*, Phys. Fluids **29**, 1509–1519 (1986)
[35] H. P. Furth, *Prevalent instability of nonthermal plasma*, Phys. Fluids **6**, 48–57 (1963)
[36] W. B. Thompson, *An introduction to plasma physics*, Addison-Wesley, Massachusetts (1962)
[37] Much of the content of Section 3C was motivated by the very constructive and focused comments of an anonymous referee, which led to significant improvement in the presentation of all the subsequent results.
[38] Zu-Yin Pu and M. G. Kivelson, *Kelvin-Helmholtz instability at the magnetopause: Solution for compressible plasmas*, J. Geophysical Res. **88**, 841–852 (1983)